Motorcycle Navigation with Two Sensors

Patrick Kessler

March 18, 2004

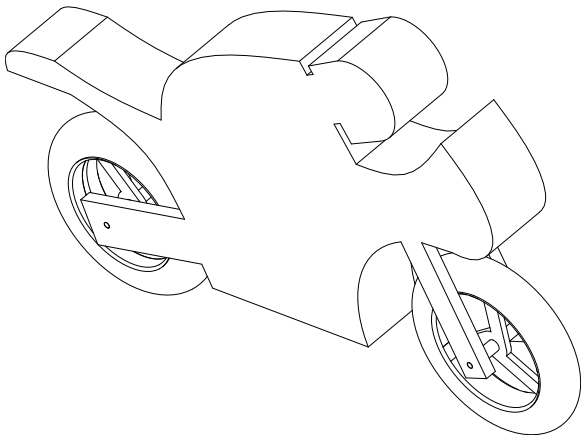

Masters Thesis
Department of Mechanical Engineering
University of California at Berkeley

Copyright © Patrick Kessler 2004

Contents

Acknowledgments

I am grateful for the guidance and support of Dr. Oliver O'Reilly in this project and in my academic journey generally. I am also grateful to Josh Coaplen, for innumerable discussions and ideas concerning motorcycles. Many people have given me valuable help on this project.

- Dr. J. Karl Hedrick served as the principal investigator during the first year and a half of the project.
- John Annany was our contact guy at BMW. Among other things, he helped Josh acquire the motorcycle velocity signal.
- Christopher Nowakowski investigated human factors issues associated with a motorcycle navigation system.
- Delphine Cody worked on human factors issues before Chris, and gave us cookies when we visited the RFS.
- Avery Jutkowitz worked on the project for about a year, obtaining a masters degree [9] based on the work he did.
- Dan Stevens also worked on the project, and obtained a masters degree [16] based on the work he did.
- Xiao Xiao is a motorcycle nut who has a lot of insight into motorcycle dynamics.

My deepest thanks to everyone, including Nathan Kinkaid who proofread my work. Also, I wish to thank the GAANN program at Berkeley, which provided me with two years of financial support, as well as Bayerische Motoren Werke AG, which made this project possible by providing a grant to the University of California at Berkeley (Award Number 014806).

1 Introduction

Vehicle navigation systems depend on multiple signals and algorithms to keep track of position. Inputs to a navigation system can include GPS (Global Positioning System) signals, compass signals, and kinematic signals (e.g., acceleration and wheel position) among others [7]. This information is fed to an algorithm that may make use of a road database to ensure that the vehicle position coincides with a known road. Information redundancy is important in navigation because it allows for the combination of the best qualities of each available signal. For example, GPS signals are accurate but relatively infrequent, while kinematic signals are always accessible but result in position errors that grow with time. An algorithm that combines these two signals can enjoy both the short term accuracy of the kinematic data and the long term accuracy of the GPS data.

In this project, we investigate the analysis of two kinematic signals from a motorcycle: forward speed, and the signal from a gyroscope mounted rigidly to the motorcycle frame. Our goal is to use these signals to obtain the position of the motorcycle as it moves over a flat surface. Improvement of the position prediction using GPS, map-matching, and other techniques is a task we leave for another day. If the kinematic signals we worked with derived from a vehicle that never tilted side to side or front to back, it would be possible in theory to use the vehicle speed and gyroscope signals to keep exact track of position. Motorcycle tracking is challenging principally because of the rolling motion that occurs when a motorcylcle executes a turn. This is illustrated in Figure 1, where kinematic signals from the same motorcycle run are fed into two algorithms, one which accounts for roll, and one which does not. The figure shows that the estimate of motorcycle position deteriorates rapidly if roll is not accounted for. Accounting for roll is obviously crucial to successful

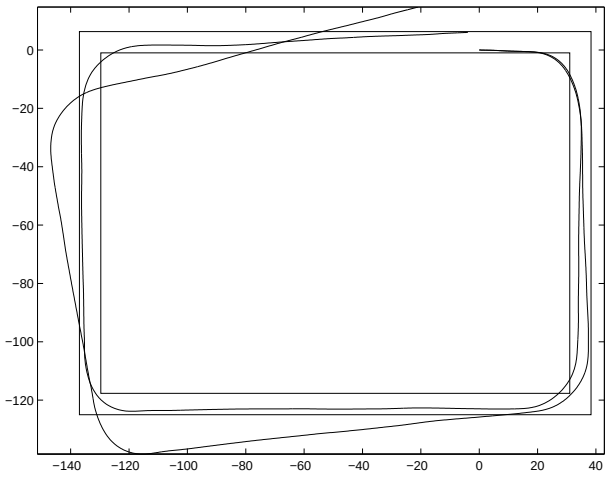

Figure 1: Axes are in meters. This figure shows path predictions for a motorcycle that travels around a typical city block. Both paths are constructed from the same speed and a gyroscope signals. The path that follows the road is generated using an algorithm of our design which accounts for motorcycle roll, while the path that wanders from the road is generated using an algorithm that does not account for roll.

motorcycle navigation, and so one of our main tasks is to find out how to do this. In the interest of economy (for possible industrial applications), we consider only the motorcycle forward speed, and the signal from a motorcycle frame mounted gyroscope. We find that a nonlinear algebraic relation maps from these signals to an estimate of the motorcycle roll, and that the error associated with this estimate is much smaller than the error associated with a direct measurement of roll (by the addition of an extra gyroscope to the motorcycle).

Once roll is known, it is possible to estimate the motorcycle path. One of our greatest challenges was coming up with a reference against which to compare this path estimate. We had hoped that by using additional sensors we would be able to generate accurate reference paths, however we found that navigation algorithms involving additional sensors were all too sensitive to signal noise and sensor error to be of any use. An extensive analysis of this sensitivity is included in Appendices D and E. The motorcycle path we generate using just two sensors follows the profile of our test track (determined using surveying tools), for

runs lasting around two minutes.

2 Project Objective

We wish to track the motion of a motorcycle over a plane given only its speed u, and the signal ω from a single axis gyroscope mounted rigidly to its frame (see Figure 2). Our main obstacle is that ω does not

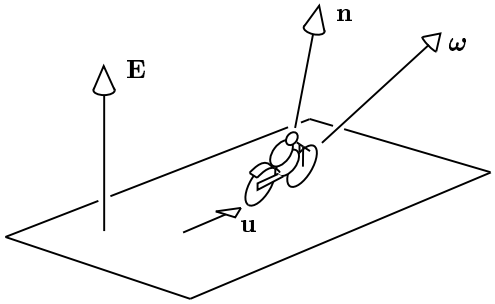

Figure 2: Shown above is a motorcycle moving over a plane. A unit vector normal to the plane is given by $\mathbf{E}$ and a unit vector fixed to the frame of the motorcycle is given by $\mathbf{n}$. The motorcycle angular velocity is given by $\boldsymbol{\omega}$, and we define $\omega = \boldsymbol{\omega} \cdot \mathbf{n}$ and $\dot{\psi} = \boldsymbol{\omega} \cdot \mathbf{E}$. The motorcycle speed u is given by the magintude of the forward pointing component of the motorcycle velocity $\mathbf{u}$.

equal the vertical component $\dot{\psi}$ of the motorcycle's angular velocity (given $\dot{\psi}$ and u, the tracking problem is trivial). For instance, in the case where the gyroscope is aligned with the upward axis of the motorcycle, ω and $\dot{\psi}$ are related by

$$\omega = \dot{\psi} \cos(\phi), \tag{1}$$

where ϕ is the motorcycle roll angle (see (A.4)). This equation is strictly true only when the motorcycle does not pitch (i.e., tilt front to back), and approximately true for standard motorcycle motions (during which pitch is small). With kinematics given by (1), the tracking problem reduces to determining the roll ϕ in terms of the two available signals u and ω.

2.1 Existence of a Solution

Although ϕ depends on additional parameters besides u and ω (such as rider movement, rider and baggage weight distribution, steering angle, road and tire traction coefficients, wind forces, $\dot{u}$ and $\dot{\omega}$, etc.), these are unavailable to us. Also, it could be that ϕ is best given implicitly as the solution to some differential equation. Our hope however is that u and ω are the dominant variables affecting ϕ, and that these map to ϕ according to some algebraic relation $\phi \approx \phi(u, \omega)$, which is accurate enough for navigational purposes. The proposal that $\phi \approx \phi(u, \omega)$ is a leap of faith, motivated by the relative complexity of other avenues of solution, such as nonlinear state observation techniques. Given any two values of u and ω, the various possible values of ϕ will range between some ϕ_{max} and some ϕ_{min}. It is useful to picture ϕ_{max} and ϕ_{min} as surfaces over (u, ω). The best any roll angle algorithm can do is to place ϕ between these surfaces. For a certain class of motions, (those with particular bounds on forward speed, side slip, rate of turning, and like quantities), the maximum error in $\phi(u, \omega)$ will be given by $E(u, \omega) = |\phi_{max}(u, \omega) \text{-} \phi_{min}(u, \omega)|$. This error will increase with the class of motions under consideration. The possibility of success in using $\phi \approx \phi(u, \omega)$ to track a motorcycle depends on whether or not the tracking error caused by E is acceptable. We will experimentally verify that tracking based on $\phi \approx \phi(u, \omega)$ results in paths that are true to actual road profiles over time intervals lasting approximately two minutes.

The question of whether or not ϕ can be determined given u and ω can also be approached using classical observability results (this was done by Dan Stevens, and is detailed in [16]). The basic idea is to construct a system model and determine whether or not an associated observability matrix satisfies certain rank

conditions. This approach is applied to nonlinear systems by linearizing about a point of interest[1]. Doing this, Stevens found that ϕ observability was possible when the motorcycle was moving forward perfectly upright ($\phi = 0$). We note that states may be unobservable but still roughly approximated to a precision accurate enough for many purposes.

3 A Simple Model

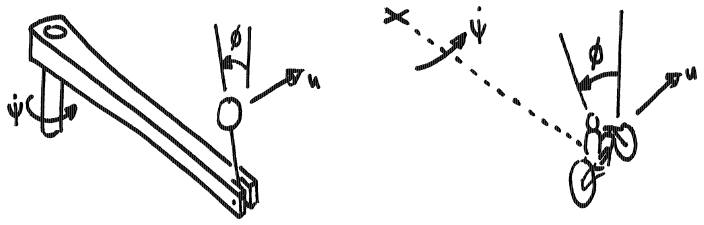

Figure 3: We propose that a rotating inverted point mass pendulum captures the essential dynamics of a motorcycle.

The actual motorcycle roll is only guaranteed to fall between the upper and lower bounding surfaces ϕ_{max} and ϕ_{min}. A roll observation scheme can place the roll estimate ϕ between these bounding surfaces in a variety of ways, for example, by interpolation on values from a look up table, or by the use of some function in the arguments u and ω. In Appendix C, we generate several such functions from very simple dynamical systems that loosely resemble a turning motorcycle. The function we end up using throughout our work is the simplest of all, consisting of an inverted point mass pendulum undergoing steady rotation. A standard analysis (see Appendix C) reveals that

$$\sin(\phi) = \lambda \frac{u\omega}{g}. \tag{2}$$

It then follows from (1) that

$$\dot{\psi} = \frac{\omega}{\sqrt{1 - (\lambda \frac{u\omega}{g})^2}}. \tag{3}$$

We found that we needed to tune the value of gravity g away from 9.8 meters/second^2, which we did with the parameter λ, (we used $\lambda = 1.1$ for every motion we tracked). The need for λ is most likely due to some dynamic effect of the motorcycle that is not accounted for by the system shown in Figure 3. As the product $u\omega$ increases to the value g/λ, the motorcycle roll angle increases from 0 to $\pi/2$. It follows that the degeneracy in (3) when $u\omega = g/\lambda$ will never be encountered under normal driving. The equilibrium position of the inverted pendulum is unstable, so the dynamics of ϕ away from its equilibrium point don't carry over to the dynamics of the motorcycle (which *is* stable under the control of a driver). A flowchart of the algorithm that follows from (3) is given below. The algorithm takes the signals u and ω as input and outputs the Cartesian coordinates x and y of the motorcycle path.

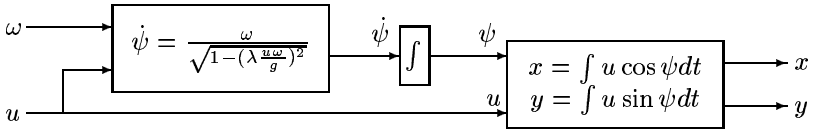

Flowchart 1: Basic Algorithm.

[1]This linearization causes conclusions not to carry over to the nonlinear system in some theoretical cases but in practice they almost always do.

4 Tracking Motorcycle Models

We now test the performance of the Basic Algorithm (Flowchart 1) by using it to track two different motorcycle models through a variety of maneuvers. (In this preliminary analysis, the models are used as stand-ins for an actual motorcycle). The first model is due to Cossalter et al. [4], and is referred to as the CDLF model after its authors. The second model is generated by Stevens [16], using the ADAMS software package. As either model is made to execute a maneuver such as rounding a corner, the resulting forward speed signal u and gyroscope signal ω are collected and fed into the Basic Algorithm (Flowchart 1). The success of the algorithm is measured by how closely its output matches the path traced out by the model. It will be seen below that the algorithm performs extremely well with both models, which we note differ significantly from each other.

4.1 Tracking the CDLF model

The CDLF model is derived from first principles in Appendix A of this report. The model consists of a rigid frame/rider mass and two tires as shown in Figure 4. A proportional control scheme realized in simulink is

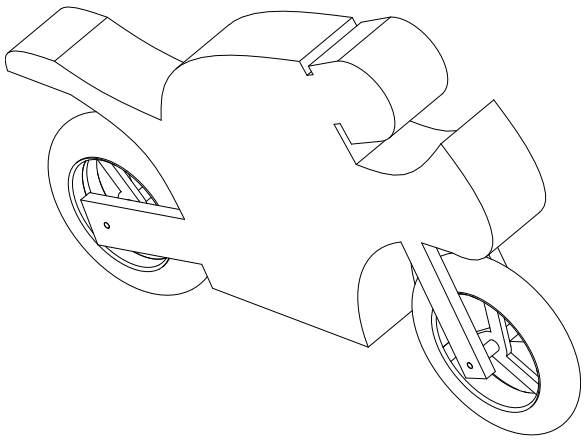

Figure 4: Diagram of the CDLF motorcycle model.

used to get the model to execute a weaving motion. The u and ω signals from this motion are then fed into the Basic Algorithm (Flowchart 1), and the resulting path is compared to the path of the model (Figure 5). The two paths are extremely close, and so the Basic Algorithm successfully tracks this motion of the CDLF model. The tracking of other CDLF model motions was equally successful.

4.2 Tracking the ADAMS model

A multibody motorcycle model was developed by Dan Stevens [16] using ADAMS software. A diagram of the model is given in Figure 6, and tracking results as it is driven around a typical city block are given in Figure 7. As with the CDLF model, the Basic Algorithm (Flowchart 1) gives excellent results.

5 Tracking Actual Data

Having verified the basic algorithm on two models, we now turn to the analysis of data from an actual motorcycle. A BMW K1200 motorcycle (see Figure 8) was instrumented with sensors[2] and driven around a 167 by 124 meter block at the Richmond Field Station (UC Berkeley) at speeds ranging from 20 to 35 km/h. Representative data from a test run is given in Figures 10 and 9. Our original plan was to use the Basic

[2]Adding instrumentation to the motorcycle and extracting signals from its native systems took a lot of work. This was accomplished by Avery Jutkowitz and Josh Coaplen, and is described in the report [8]. We used the Crossbow IMU300CC-100 sensor package of three accelerometers and three gyroscopes to take part of our data.

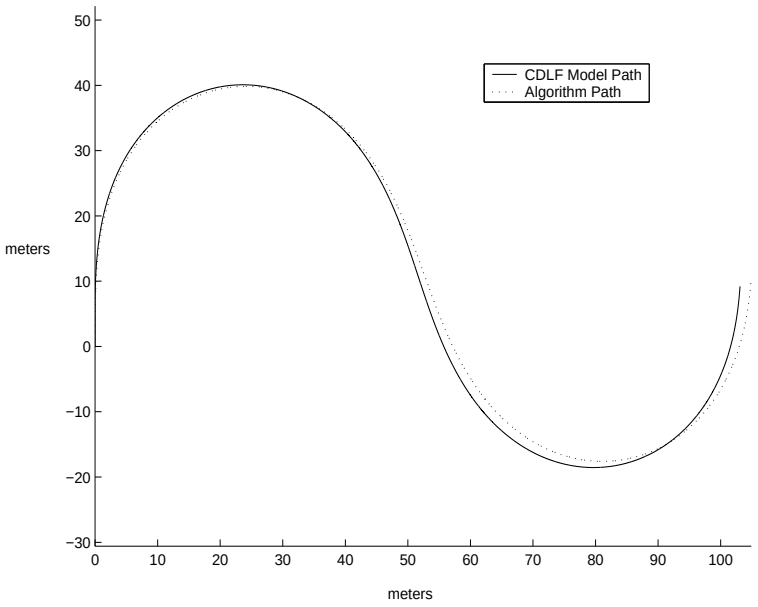

Figure 5: Tracking results for the CDLF Model. A set of time varying states is fed into the CDLF model as realized in Simulink. These cause the model to trace out a path (shown as a solid line). Over this path, the speed u is approximately 9 meters/second, and the maximum roll angle ϕ is 25°. Given u and ω, the Basic Algorithm (Flowchart 1) predicts a path (shown as a dashed line). The fact that the two paths are almost indistinguishable shows that the Basic Tracking Algorithm performs very well.

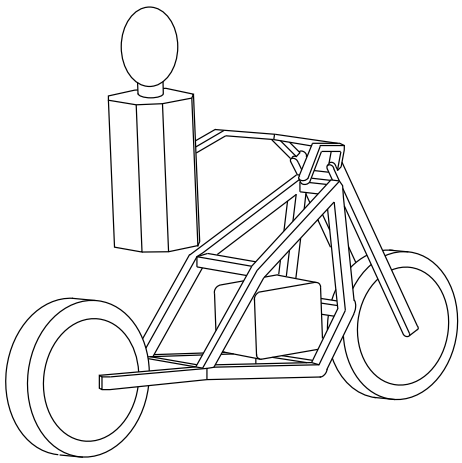

Figure 6: Diagram of the multi-body motorcycle model constructed using ADAMS.

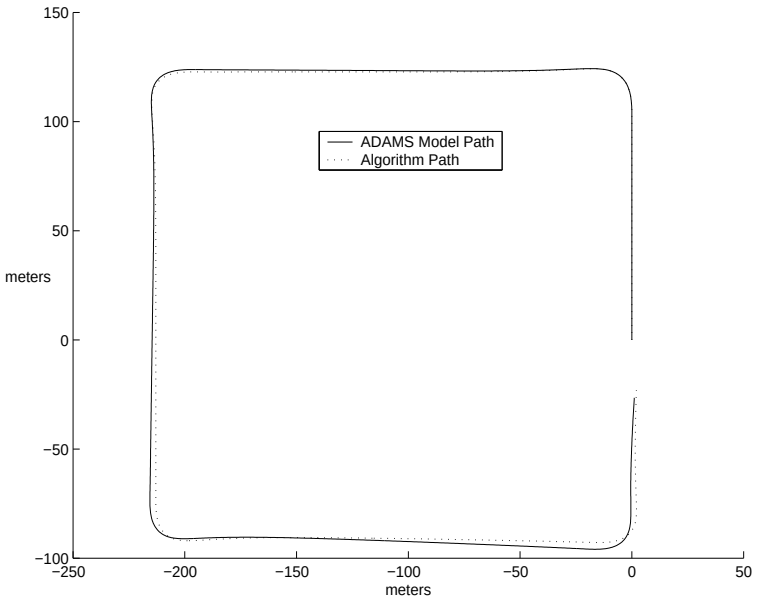

Figure 7: Tracking results for the ADAMS Model. The model is made to drive around a city block as detailed in [16]. During this motion, the model speed u varies from 6 meters/second during turns to 10.5 meters/second along the straightaways, and the roll angle ϕ reaches a maximum of 20° during turns. The path predicted by the Basic Algorithm in Flowchart 1 is shown as a dashed line, and as with the CDLF model, matches the actual model path very closely.

Figure 8: This is the BMW K1200 motorcycle we used for our tests.

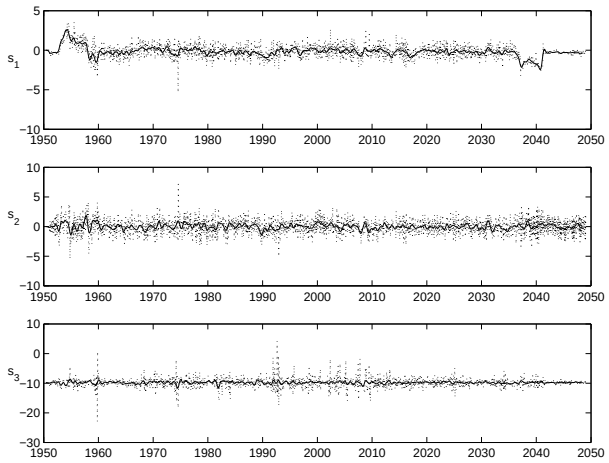

Figure 9: This is a generic set of accelerometer data (in units of meters/seconds^2 versus seconds), taken as the motorcycle was driven around a 167 by 124 meter block at the Richmond Field Station. The dotted line shows raw data and the solid line shows the result of passing this data through a Butterworth filter.

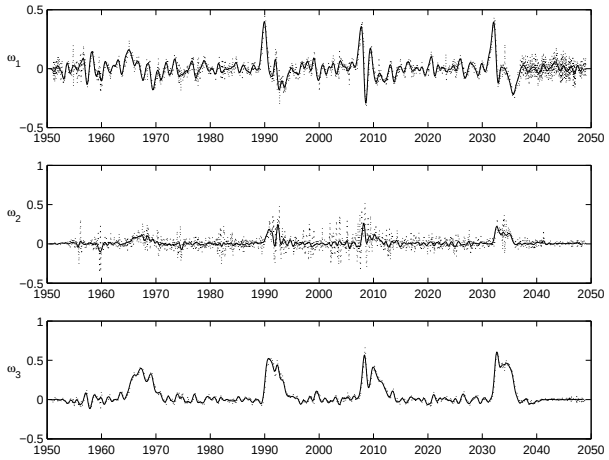

Figure 10: This is gyroscope signal data (in units of radians/second versus seconds), taken during the same run as the accelerometer data in Figure 9. As in Figure 9, we superpose raw and filtered signals, shown as dotted and solid lines respectively.

Algorithm in Flowchart 1 to generate a path given the motorcycle's forward speed and the signal from an upward pointing gyroscope fixed to the motorcycle, and to compare this path to an accurate reference path generated using signals from an array of three accelerometers and three gyroscopes. As it turned out, the path generated by the Basic Algorithm was more accurate than any path we could construct using additional sensor signals. To construct a reference against which to judge the Basic Algorithm, we resorted to a careful measurement of the test track using optical surveying devices.

5.1 A Complete Navigation Algorithm

The general problem of navigating with three accelerometer and three gyroscope signals is discussed in Appendix D. The calculations needed to get from the sensor signals to a set of inertial frame velocity values and Euler angles are complicated and involve feedback that renders them extremely sensitive to accelerometer and gyroscope noise and bias. These calculations are shown in the Complete Algorithm (Flowchart 2 below) from Appendix D.

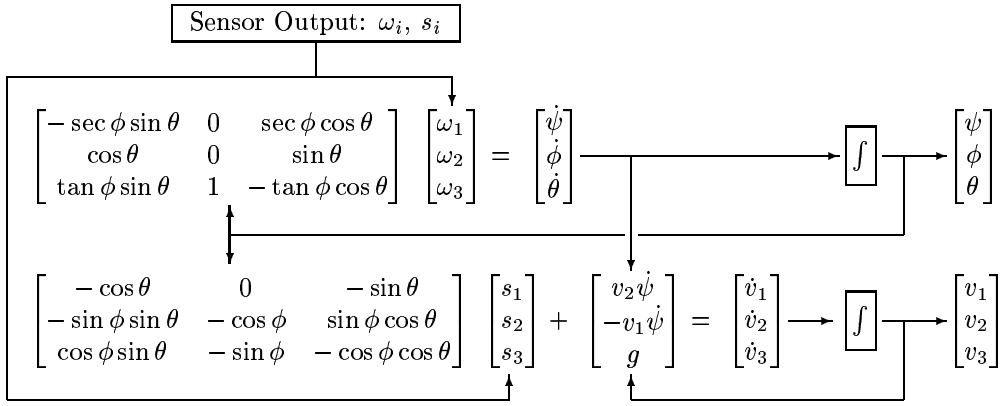

Flowchart 2: The Complete Algorithm.

We find that this algorithm is too sensitive for the data from our sensors. Our fundamental problem is integration error. Roughly speaking, input signal bias of magnitude C is reflected in the output of a calculation involving n series integrations as an error term with the form Ct^n. Feeding integration results back into the integral results in error terms of the form Ce^t. The bias in our sensors is such that the output of the Complete Algorithm becames nonsensical after only a second or two while the maneuvers we are interested in tracking last at least several seconds.

5.2 A Simplified Algorithm

After becoming aware of the difficulties with using the Complete Algorithm, we searched for ways to simplify our calculations. In hindsight, something as general as the Complete Algorithm (which accommodates motions as complicated as that of a body tumbling through space) is inappropriate for the simpler motion of a motorcycle[3]. The fact that a motorcycle generally maintains contact with the (level) ground and pitches very little gives us constraints with which to simplify the navigation process. For instance, in the error analysis of the Complete Algorithm (in Appendix D), we note that velocity error is dramatically reduced by not accounting for side slip, vertical components of the motion, or pitch, all of which are nominally zero. After these changes, the navigation process reduces to the Simplified Algorithm, shown in Flowchart 3.

[3]All signals are noisy and biased, and algorithm sensitivity to noise and bias increases as the number of integrations in the algorithm increases; for practical engineering it is generally a good idea to make things as simple as possible.

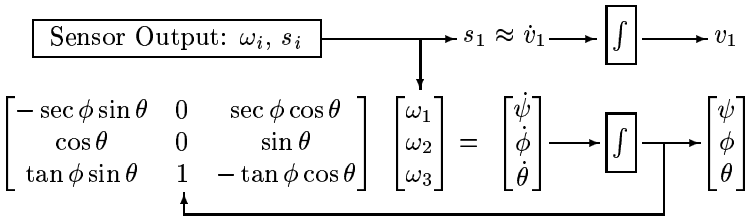

Flowchart 3: The Simplified Algorithm.

Even after this simplification, bias in the signal from the forward pointing accelerometer caused its integral (our velocity signal) to quickly become unreasonable (see Figure 11), and to get a meaningful velocity signal (Figure 11), and meaningful Euler angles (Figure 12), we had to post-process our data. We justified these

Figure 11: Velocity profile constructed from data in Figures 10 and 9. The dotted line is our initial result, obtained by integrating the filtered signal from the forward pointing accelerometer. We know that the motorcycle is stationary at the beginning and end of an interval of forward motion, so we apply a linear adjustment to the dotted line to get the reasonable velocity signal shown as a solid line. We also know that the motorcycle is at rest before and after the middle part of the test run, so we set the velocity to zero during these periods.

adjustments by the fact that bias was apparent in our data and that they resulted in output signals closer to the motorcycle motion we observed during a test run. Had the resources been available to invest in more expensive sensors, they likely would have provided signals closer to our adjusted signals.

5.3 Testing the Basic Algorithm by Visual Inspection

The trend of improved performance with algorithm simplification does not stop with the Simplified Algorithm in Flowchart 3. Evidence that the Basic Algorithm which we set out to test in the first place outperforms the Simplified Algorithm is given in Figure 13. In this Figure, the motorcycle roll as calculated by the Simplified Algorithm wanders from zero during straight forward portions of the motorcycle run while the magnitude of the roll predicted by the Basic Algorithm does not (we observed that the actual motorcycle roll was very close to zero during these portions of the testing).

Coming up empty handed in our search for a standard against which to compare the Basic Algorithm[4], we used optical surveying instruments to measure the rectangular motorcycle test track, which we find to be 167 meters by 124 meters, with a width of 7.3 meters. We then superposed an image of this track on the output path of the Basic Algorithm, as shown in Figure 15. The quality of the Basic Algorithm is measured

[4]A real time GPS signal recorder might have served this purpose.

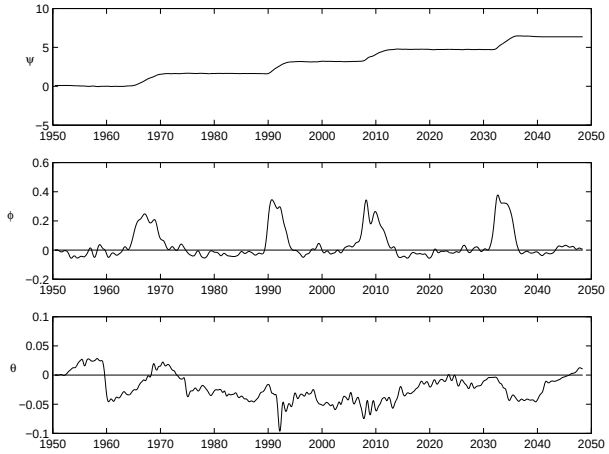

Figure 12: Euler angles (in radians) as functions of time (in seconds), recovered from the filtered gyroscope signals in Figure 10, after adding small constant values to correct for sensor bias. Note the difference in scale between the plots.

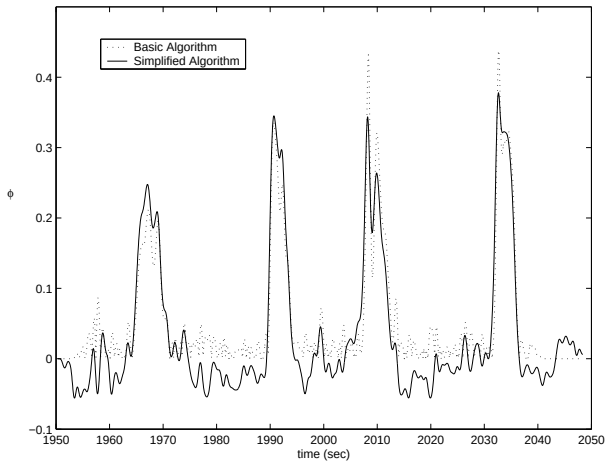

Figure 13: This Figure superposes the roll signal from the middle graph of Figure 12 (shown here as a solid line), and the magnitude of the roll angle ϕ predicted by the Basic Algorithm from Flowchart 1 (shown as a dotted line). The graph units are radians versus seconds. During straight line portions of the test, the motorcycle roll angle is approximately zero. With respect to this important aspect of the motion, the results of the Basic Algorithm are closer to the actual motion of the motorcycle than the roll angle predicted by Flowchart 3.

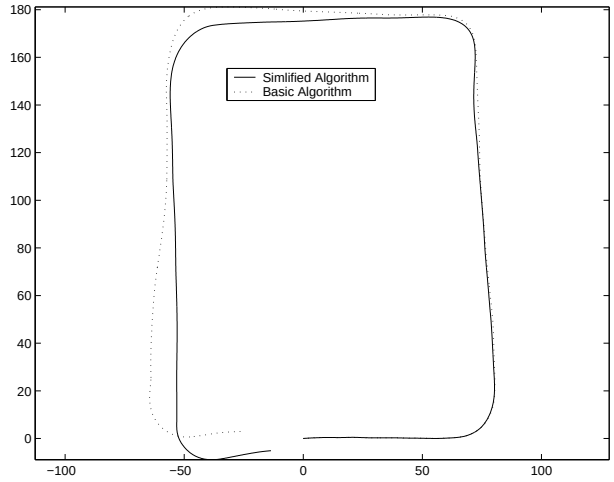

Figure 14: This Figure compares the paths generated by the Basic Algorithm in Flowchart 1 and the Simplified Algorithm in Flowchart 3. The Figure axes are in meters. Both paths are constructed using the corrected velocity signal (from Figure 11), and the Euler angles shown in Figure 12. Both paths exhibit the same order of accuracy, and so it is inappropriate to use one as a basis for judging the other.

by how well its output remains on the motorcycle test track. Although there is consistent corner cutting which we have been unable to explain, the Basic Algorithm outputs a path that stays true to the test track for runs lasting as long as several minutes.

A good velocity signal is instrumental in generating the results shown in Figure 15. Although seemingly a straightforward matter of tapping into the motorcycle's circuitry for the wheel position signal, obtaining a good velocity signal proved challenging[5]. It is interesting to compare the velocity signal from the motorcycle circuitry to the integral of the forward pointing accelerometer (see Figure 16).

5.4 Refining the Basic Algorithm

In this section we note a refinement of the Basic Algorithm that is explained in detail in Appendix E. In our refinement we take into account the fact that velocity will usually be computed from wheel position data, and that minor improvements in performance are possible if the roll of the motorcycle is accounted for when these computations are performed. These changes are reflected in Flowchart 4 below, where ω_3 is a gyroscope signal and t_i is a stream of discrete time values, each corresponding to an angular increment Φ in the position of the rear motorcycle wheel.

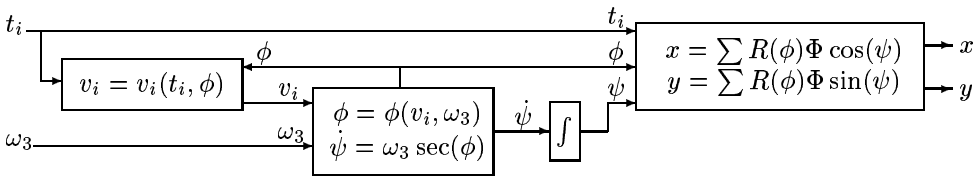

Flowchart 4: The Refined Algorithm.

6 Conclusions and Further Work

Our motorcycle tracking goal is accomplished, as we have generated an algorithm that produces paths true to actual motorcycle trajectories over time intervals lasting a couple of minutes. The algorithm does not

[5]For details on the circuit needed to obtain the speedometer signal, see the report [8]

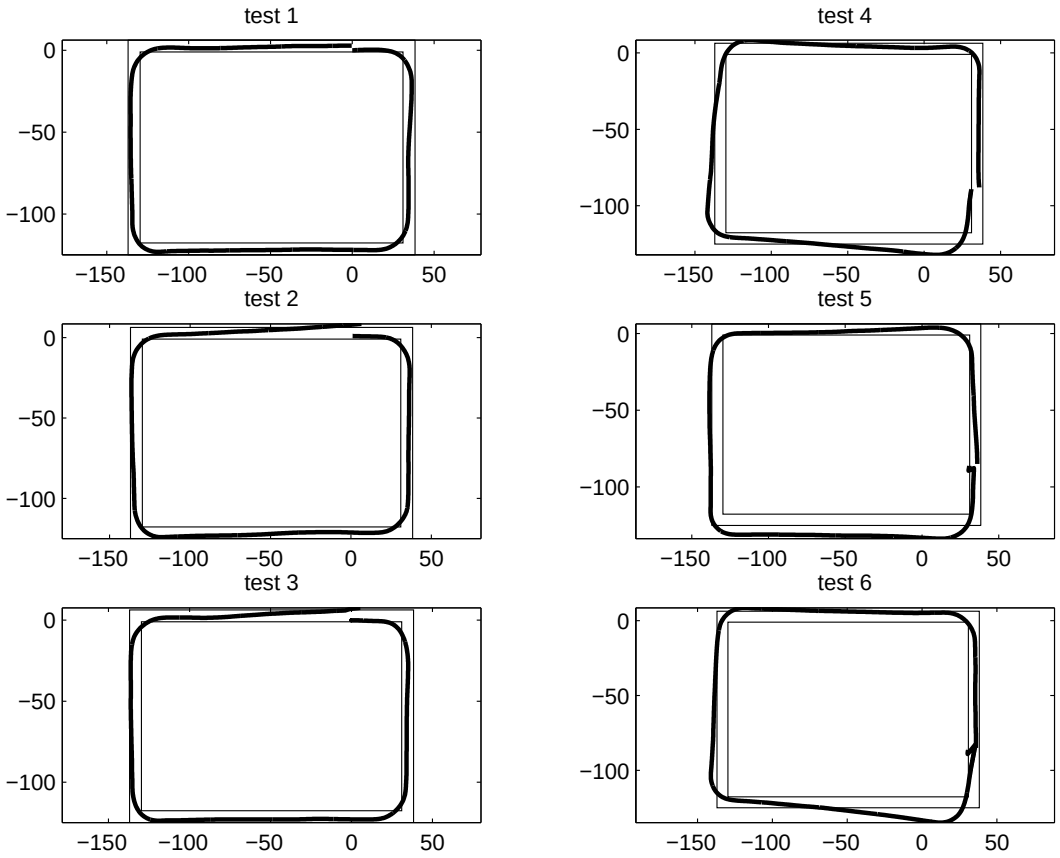

Figure 15: Basic Algorithm tracking results for the BMW K1200 motorcycle as it is driven around the test block at the Richmond Field Station. In the three tests on the left the motorcycle is driven clockwise (as seen from above) while in the three tests on the right, the motorcycle is driven counter-clockwise. In all cases the motorcycle speed was roughly 7 meters/second. In every case, ω is corrected for bias by subtracting the average of ω over a small initial time interval from the entire signal. (Over this interval, ω should be approximately zero due to lack of motion by the motorcycle). The velocity v is measured directly using Coaplen's circuit.

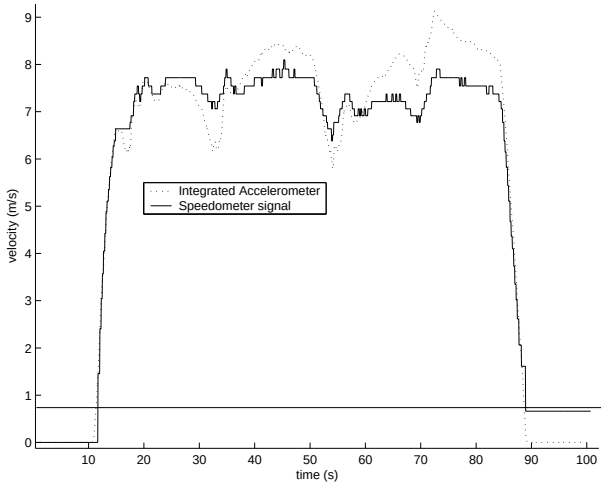

Figure 16: A comparison of the velocity signal from Coaplen's circuit (solid line) to the velocity signal obtained from the forward pointing accelerometer (dotted line). A linear correction has been applied to the dotted line, similar to the one shown in Figure 11. The signal from Coaplen's circuit is closest to the velocity observed by the motorcycle rider. We note that Coaplen's circuit sometimes returns a residual velocity signal after the motorcycle has come to rest (as shown above). This effect is discussed in [8].

depend on parameters such as the motorcycle mass and traction coefficients, and so it is robust to variability in these quantities. Because it involves no integration, the algorithm prediction of roll is better than direct measurement of roll using a forward pointing gyroscope.

Further work on this project could be done to extend the algorithm to non-flat surfaces, and to implement the algorithm in real time (a step in this direction is given by the Refined Algorithm in Flowchart 4). Performance might be improved by using a set of correction factors that are activated at different rates and speeds (i.e., $\lambda = \lambda(u, \omega)$). It seems likely that λ at very low speeds will differ from λ at very high speeds, because at low speeds, steering geometry becomes more important, (and the motorcycle acts less like an inverted pendulum). These and other algorithm improvements will be difficult to study without knowledge of the actual motorcycle trajectory. Although the surveying techniques we used were sufficient for us to draw important conclusions, the reference trajectories we constructed were perfect rectangles, and omitted details of the motorcycle motion during a turn. Improvements in trajectory resolution could be achieved using real time GPS corrections. This however is an entire set of pandora's boxes, enough to fuel several masters projects.

Josh Coaplen and I have noted a paradigm shift appropriate when INS is used in conjunction with map matching. Instead of providing position estimates in the short term that are corrected periodically by signals from GPS, the INS would only need to make available the total distance traveled, in a direction given by the road or freeway the motorcycle is known to be traveling on. This total distance would be the integral of the speedometer signal (equivalently a summation of wheel position counts), mitigated by the amount of weaving the vehicle does (measured by the upward pointing gyroscope). Of course, when an intersection or road fork is anticipated (by the map matching software), INS would switch to provide full short term position output.

A Dynamic Model of a Motorcycle

This model follows V. Cossalter et al. [4], and is referred to in this report as the CDLF model.

A.1 Overview

Our model consists of two wheels pivoted to a rigid frame which includes the motorcycle rider. Frame compliance (shocks) and in particular steering are neglected. The traction between the tires and the road does not follow easily from traditional control inputs such as steering torque and slight shifts in driver weight, so we use traction resultants directly as inputs, and assume that the driver is able to create them. We note

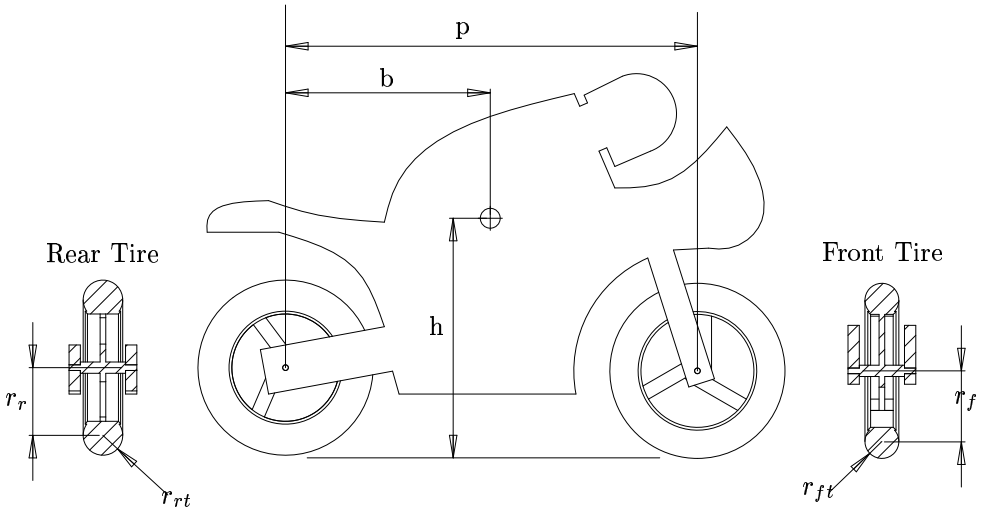

Figure 17: Schematic of the motorcycle model.

that in Figure 17, frame dimensions are taken with respect to the center of mass of a collection of three bodies: the motorcycle frame/rider, the front tire, and the rear tire.

A.2 Tires

The tires in our model determine the position and orientation of the motorcycle as if they were infinitly thin rigid disks. Traction forces and moments are applied to the tires at points in the plane of the road as shown in Figure 18. Justification for neglecting tire thickness in the model kinematics follows from the

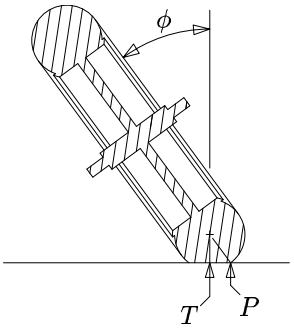

Figure 18: Here we illustrate our assumptions about how the motorcycle tire contacts the ground. Changing ϕ causes the tire to pivot about the point P as if hinged there. Traction forces are applied at point T, which is a distance $r \sin \phi$ from P, (with r the minor radius of the toroidal tire).

small change in position of the base point of a rigid torus as the torus rolls without slipping in its facewise direction through an angle ϕ (see Figure 19). Note that e_x and e_y are both very small (e_x is $O(r\phi^3)$ and e_y

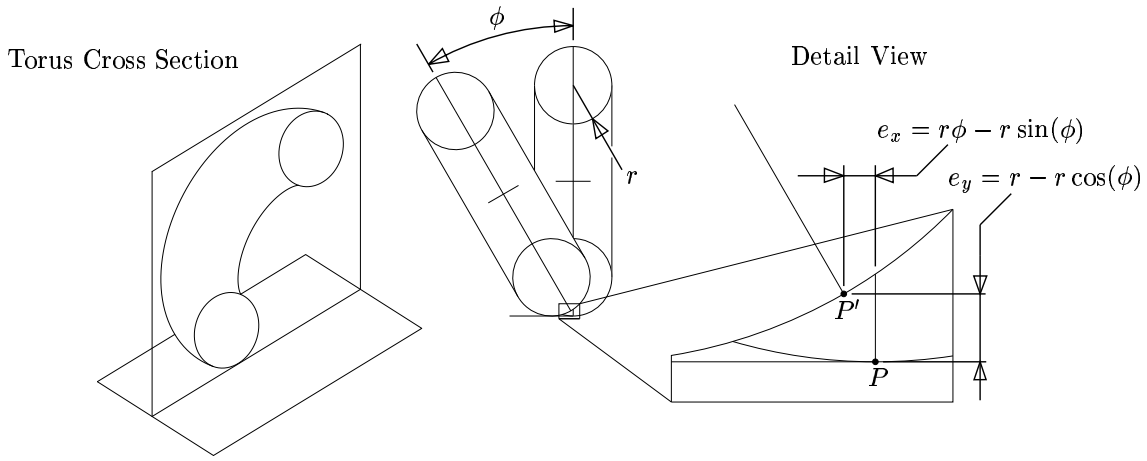

Figure 19: When $\phi = 0$, the torus contacts the ground at point P. In the diagram above, the torus rolls over the ground as ϕ increases. The difference between this rolling and simple pivoting of the torus about P is measured by e_x and e_y.

is $O(r\phi^2)$), and that when the torus is compliant (as it is with a real motorcycle tire), e_y is reduced further still. Although tire thickness can be neglected in the model kinematics, it must be accounted for in the location of the traction resultants. The lateral displacement value $r\sin\phi$ was chosen because it locates the point of contact of a rigid torus with the ground (as shown in Figure 19).

A.3 Bases

A body fixed basis $\{\mathbf{b}_i\}$ is defined using the fixed basis $\{\mathbf{E}_i\}$. The vector $\mathbf{E}_3$ points down; a yaw rotation ψ about $\mathbf{E}_3$ gives the basis $\{\mathbf{a}_i\}$; a roll rotation ϕ about $\mathbf{a}_1$ gives the basis $\{\mathbf{b}_i\}$. The vector $\mathbf{b}_1$ points in the forward direction of the motorcycle and is horizontal.

$$\begin{bmatrix}\mathbf{a}_1\\ \mathbf{a}_2\\ \mathbf{a}_3\end{bmatrix} = \begin{bmatrix}\cos(\psi) & \sin(\psi) & 0\\ -\sin(\psi) & \cos(\psi) & 0\\ 0 & 0 & 1\end{bmatrix}\begin{bmatrix}\mathbf{E}_1\\ \mathbf{E}_2\\ \mathbf{E}_3\end{bmatrix}, \tag{A.1}$$

$$\begin{bmatrix}\mathbf{b}_1\\ \mathbf{b}_2\\ \mathbf{b}_3\end{bmatrix} = \begin{bmatrix}1 & 0 & 0\\ 0 & \cos(\phi) & \sin(\phi)\\ 0 & -\sin(\phi) & \cos(\phi)\end{bmatrix}\begin{bmatrix}\mathbf{a}_1\\ \mathbf{a}_2\\ \mathbf{a}_3\end{bmatrix}. \tag{A.2}$$

Whence we see that

$$\begin{bmatrix}\mathbf{b}_1\\ \mathbf{b}_2\\ \mathbf{b}_3\end{bmatrix} = \begin{bmatrix}\cos(\psi) & \sin(\psi) & 0\\ -\cos(\phi)\sin(\psi) & \cos(\phi)\cos(\psi) & \sin(\phi)\\ \sin(\phi)\sin(\psi) & -\sin(\phi)\cos(\psi) & \cos(\phi)\end{bmatrix}\begin{bmatrix}\mathbf{E}_1\\ \mathbf{E}_2\\ \mathbf{E}_3\end{bmatrix}. \tag{A.3}$$

A.4 Angular Velocities

The angular velocity of the motorcycle frame is given by

$$\begin{aligned}\boldsymbol{\omega} &= \dot{\phi}\mathbf{b}_1 + \dot{\psi}\mathbf{E}_3\\ &= \dot{\phi}\mathbf{b}_1 + \dot{\psi}\sin(\phi)\mathbf{b}_2 + \dot{\psi}\cos(\phi)\mathbf{b}_3.\end{aligned} \tag{A.4}$$

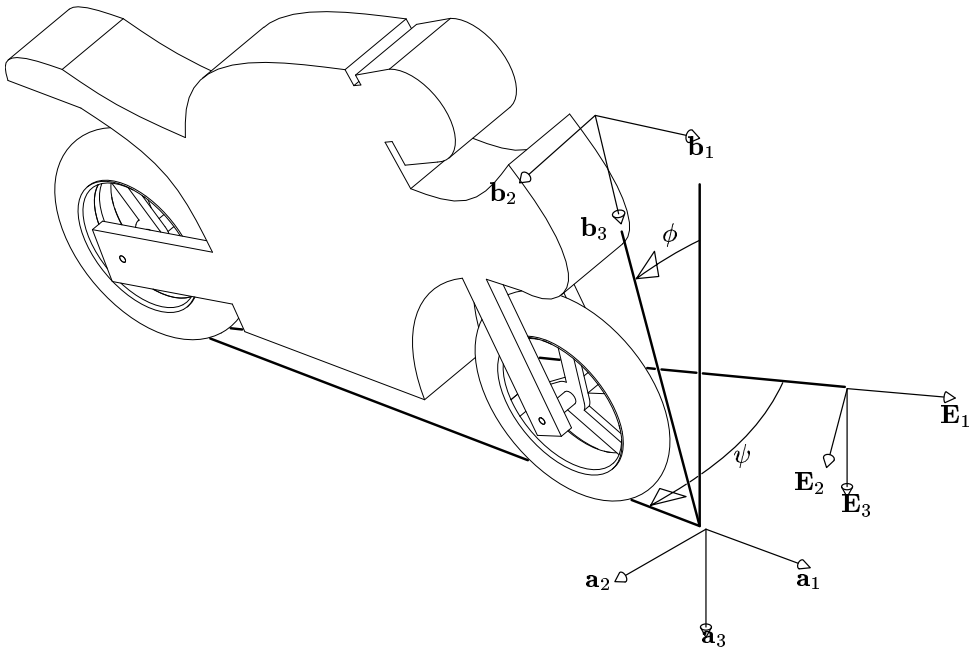

Figure 20: Illustration of various bases and angles used in the model.

In prescribing the front and rear wheel angular velocities, $\boldsymbol{\omega}_f$ and $\boldsymbol{\omega}_r$ respectively, we assume rolling without slipping of the tires in the $\mathbf{b}_2$ direction. Note however that sliding in the $\mathbf{a}_2$ direction is not prohibited as the velocity of the rear wheel contact point can have an $\mathbf{a}_2$ component.

$$\begin{aligned}\boldsymbol{\omega}_f &= \boldsymbol{\omega} - \frac{u}{r_f + r_{ft}}\mathbf{b}_2 \text{ (front wheel)},\\ \boldsymbol{\omega}_r &= \boldsymbol{\omega} - \frac{u}{r_r + r_{rt}}\mathbf{b}_2 \text{ (rear wheel)}.\end{aligned} \tag{A.5}$$

In this model, we neglect the change in effective tire radius with roll of the motorcycle.

A.5 Preliminaries

In the development that follows, we'll need $\{\dot{\mathbf{b}}_i\}$ and $\{\ddot{\mathbf{b}}_i\}$. Because $\{\dot{\mathbf{b}}_i\}$ is body fixed, $\dot{\mathbf{b}}_i = \boldsymbol{\omega} \times \mathbf{b}_i$:

$$\begin{aligned}\dot{\mathbf{b}}_1 &= \dot{\psi}\cos(\phi)\mathbf{b}_2 - \dot{\psi}\sin(\phi)\mathbf{b}_3,\\ \dot{\mathbf{b}}_2 &= -\dot{\psi}\cos(\phi)\mathbf{b}_1 + \dot{\phi}\mathbf{b}_3,\\ \dot{\mathbf{b}}_3 &= \dot{\psi}\sin(\phi)\mathbf{b}_1 - \dot{\phi}\mathbf{b}_2.\end{aligned} \tag{A.6}$$

The rates $\{\ddot{\mathbf{b}}_i\}$ follow easily:

$$\begin{aligned}\ddot{\mathbf{b}}_1 = {}& \mathbf{b}_1(-\dot{\psi}^2)\\ &+ \mathbf{b}_2(\ddot{\psi}\cos(\phi))\\ &+ \mathbf{b}_3(-\ddot{\psi}\sin(\phi)),\end{aligned} \qquad \begin{aligned}\ddot{\mathbf{b}}_2 = {}& \mathbf{b}_1(2\dot{\psi}\dot{\phi}\sin(\phi) - \ddot{\psi}\cos(\phi))\\ &+ \mathbf{b}_2(-\dot{\phi}^2 - \dot{\psi}^2\cos^2(\phi))\\ &+ \mathbf{b}_3(\ddot{\phi} + \dot{\psi}^2\sin(\phi)\cos(\phi)),\end{aligned}$$

$$\begin{aligned}\ddot{\mathbf{b}}_3 = {}& \mathbf{b}_1(\ddot{\psi}\sin(\phi) + 2\dot{\psi}\dot{\phi}\cos(\phi))\\ &+ \mathbf{b}_2(-\ddot{\phi} + \dot{\psi}^2\sin(\phi)\cos(\phi))\\ &+ \mathbf{b}_3(-\cot\phi^2 - \dot{\psi}^2\sin^2(\phi)).\end{aligned} \tag{A.7}$$

A.6 Overview of the Dynamics

We model the motorcycle as a collection of three essentially rigid bodies (i.e., the frame and the two tires). The dynamics of our model are developed with respect to $\mathbf{x}$, the center of mass of this collection, and follow from standard balances of linear and angular momentum. The forces and moments acting on the motorcycle are:

$$\begin{aligned}
\mathbf{S}_f &= S_f \mathbf{b}_1 \text{ the forward force acting on the front tire,} \\
\mathbf{S}_r &= S_r \mathbf{b}_1 \text{ the forward force acting on the rear tire,} \\
\mathbf{F}_f &= F_f \mathbf{a}_2 \text{ the lateral force acting on the front tire,} \\
\mathbf{F}_r &= F_r \mathbf{a}_2 \text{ the lateral force acting on the rear tire,} \\
\mathbf{N}_f &= -N_f \mathbf{a}_3 \text{ the vertical force acting on the front tire,} \\
\mathbf{N}_r &= -N_r \mathbf{a}_3 \text{ the vertical force acting on the rear tire,} \\
\mathbf{M}_f &= M_f \mathbf{a}_3 \text{ the moment acting on the front tire,} \\
\mathbf{M}_r &= M_r \mathbf{a}_3 \text{ the moment acting on the rear tire,} \\
\mathbf{F}_a &= -F_a \mathbf{b}_1 \text{ the aerodynamic drag force,} \\
\mathbf{F}_g &= mg\mathbf{a}_3 \text{ the gravitational body force.}
\end{aligned} \tag{A.8}$$

Keep in mind that the *motorcycle* is a collection of three rigid bodies; the mass m for instance in $\mathbf{F}_g$ is the sum of the masses of each of three bodies. As noted in the overview, the forces $\mathbf{S}_f$, $\mathbf{S}_r$, and $\mathbf{F}_f$ are control inputs for the model. The moments on the tires are dominated by their $\mathbf{a}_3$ components.

A.6.1 A Balance of Linear Momentum

A balance of linear momentum is given by

$$\mathbf{F} = m\ddot{\mathbf{x}}, \tag{A.9}$$

where

- $\mathbf{F}$ is the sum of all external forces acting on the motorcycle,
- m is the mass of the motorcycle,
- $\ddot{\mathbf{x}}$ is the acceleration of the motorcycle's center of mass.

We denote the velocity of the rear wheel kinematical contact point with the ground by $\mathbf{v} = u\mathbf{a}_1 + v\mathbf{a}_2$. It follows that

$$\dot{\mathbf{x}} = u\mathbf{b}_1 + v(\cos(\phi)\mathbf{b}_2 - \sin(\phi)\mathbf{b}_3) - h\dot{\mathbf{b}}_3 + b\dot{\mathbf{b}}_1. \tag{A.10}$$

This vector can be differentiated:

$$\begin{aligned}
\ddot{\mathbf{x}} = {} & \mathbf{a}_1(\dot{u} - \dot{\psi}v - b\dot{\psi}^2 - h\ddot{\psi}\sin(\phi) - 2h\dot{\psi}\dot{\phi}\cos(\phi)) \\
& + \mathbf{a}_2(u\dot{\psi} + \dot{v} + b\ddot{\psi} + h\ddot{\phi}\cos(\phi) - h\dot{\phi}^2\sin(\phi) - h\dot{\psi}^2\sin(\phi)) \\
& + \mathbf{a}_3(h\ddot{\phi}\sin(\phi) + h\dot{\phi}^2\cos(\phi)).
\end{aligned} \tag{A.11}$$

Resolving $\mathbf{F}$ against the $\{\mathbf{a}_i\}$ basis and equating components with $m\ddot{\mathbf{x}}$, we find that

$$\begin{aligned}
S_f + S_r - F_a &= m(\dot{u} - \dot{\psi}v - b\dot{\psi}^2 - h\ddot{\psi}\sin(\phi) - 2h\dot{\psi}\dot{\phi}\cos(\phi)), \\
F_f + F_r &= m(u\dot{\psi} + \dot{v} + b\ddot{\psi} + h\ddot{\phi}\cos(\phi) - h\dot{\phi}^2\sin(\phi) - h\dot{\psi}^2\sin(\phi)), \\
mg - N_f - N_r &= m(h\ddot{\phi}\sin(\phi) + h\dot{\phi}^2\cos(\phi)).
\end{aligned} \tag{A.12}$$

A.6.2 A Balance of Angular Momentum

A balance of angular momentum is given by

$$\mathbf{M} = \frac{d}{dt}\left(\mathbf{J}_F\boldsymbol{\omega} \ + \mathbf{J}_r\boldsymbol{\omega}_r \ + \mathbf{J}_f\boldsymbol{\omega}_f \ + \tilde{\mathbf{J}}\tilde{\boldsymbol{\omega}}\right), \tag{A.13}$$

where $\mathbf{M}$ is the net external moment on the motorcycle with respect to $\mathbf{x}$. The symbols $\mathbf{J}_F$, $\mathbf{J}_r$, and $\mathbf{J}_f$ respectively denote the inertia tensors of the frame, the rear wheel, and the front wheel about their respective centers of mass. As discussed in Appendix B, $\tilde{\mathbf{J}}$ is given by

$$\tilde{\mathbf{J}} = \sum m_i(\mathbf{I}(\boldsymbol{\pi}_i \cdot \boldsymbol{\pi}_i - \boldsymbol{\pi}_i \otimes \boldsymbol{\pi}_i)), \tag{A.14}$$

with summation over $i \in \{F, r, f\}$. The vector $\boldsymbol{\pi}_i$ goes from the center of mass of all three rigid bodies to the center of mass of the i^{th} rigid body, and m_i is the mass of the i^{th} rigid body. The wheel centers of mass are indistinguishable from motorcycle frame material points, and so $\tilde{\boldsymbol{\omega}} = \boldsymbol{\omega}$. Furthermore, $\mathbf{b}_2$ is a principle axis of both $\mathbf{J}_F$ and $\tilde{\mathbf{J}}$, so letting $\mathbf{J}$ denote the sum of $\mathbf{J}_F$ and $\tilde{\mathbf{J}}$, we have $\mathbf{J}_F\boldsymbol{\omega} + \tilde{\mathbf{J}}\tilde{\boldsymbol{\omega}} = \mathbf{J}\boldsymbol{\omega}$ where the components of $\mathbf{J}$ with respect to the $\{\mathbf{b}_i \otimes \mathbf{b}_j\}$ basis are given by

$$\mathbf{J} = \begin{bmatrix} J_1 & 0 & J_4 \\ 0 & J_2 & 0 \\ J_4 & 0 & J_3 \end{bmatrix}_{\mathbf{b}_i \otimes \mathbf{b}_j}. \tag{A.15}$$

With these changes, (A.13) becomes

$$\mathbf{M} = \frac{d}{dt}\left(\mathbf{J}\boldsymbol{\omega}\right) \ - \frac{d}{dt}\left(\frac{uI_{er}}{r_r + r_{rt}}\mathbf{b}_2\right) \ - \frac{d}{dt}\left(\frac{uI_{ef}}{r_f + r_{ft}}\mathbf{b}_2\right), \tag{A.16}$$

where I_{er} and I_{ef} denote the rear and front wheel moments of inertia respectively about their axes of symmetry. The vectors $\mathbf{k}_r$ and $\mathbf{k}_f$ going from $\mathbf{x}$ to the rear and front wheel points of force application respectively are given by

$$\begin{aligned} \mathbf{k}_r &= r_{rt}\sin(\phi)\cos(\phi)\mathbf{b}_2 - b\mathbf{b}_1 - (r_{rt} - r_{rt}\cos^2(\phi) - h)\mathbf{b}_3, \\ \mathbf{k}_f &= r_{ft}\sin(\phi)\cos(\phi)\mathbf{b}_2 + (p - b)\mathbf{b}_1 - (r_{ft} - r_{ft}\cos^2(\phi) - h)\mathbf{b}_3. \end{aligned} \tag{A.17}$$

The net external moment $\mathbf{M}$ on the motorcycle is therefore given by

$$\begin{aligned} \mathbf{M} &= \mathbf{M}_r + \mathbf{M}_f + \mathbf{k}_r \times (\mathbf{S}_r + \mathbf{F}_r + \mathbf{N}_r) + \mathbf{k}_f \times (\mathbf{S}_f + \mathbf{F}_f + \mathbf{N}_f) \\ &= \mathbf{b}_1((r_{rt} - h)(F_r\cos(\phi) - N_r\sin(\phi)) - r_{rt}F_r\cos(\phi)\ldots \\ &\qquad + (r_{ft} - h)(F_f\cos(\phi) - N_f\sin(\phi)) - r_{ft}F_f\cos(\phi)) \\ &\quad + \mathbf{b}_2((M_r + M_f)\sin(\phi)\ldots \\ &\qquad + S_r(h - r_{rt} + r_{rt}\cos^2(\phi)) - b(F_r\sin(\phi) + N_r\cos(\phi))\ldots \\ &\qquad + S_f(h - r_{ft} + r_{ft}\cos^2(\phi)) - (b - p)(F_f\sin(\phi) + N_f\cos(\phi))) \\ &\quad + \mathbf{b}_3((M_r + M_f)\cos(\phi)\ldots \\ &\qquad - b(F_r\cos(\phi) - N_r\sin(\phi)) - S_r r_{rt}\sin(\phi)\cos(\phi)\ldots \\ &\qquad - (b - p)(F_f\cos(\phi) - N_f\sin(\phi)) - S_f r_{ft}\sin(\phi)\cos(\phi)). \end{aligned} \tag{A.18}$$

Expanding the right side of (A.16) gives

$$\begin{aligned} \mathbf{M} &= \mathbf{b}_1(J_1\ddot{\phi} + J_4\ddot{\psi}\cos(\phi) + (J_3 - J_2)\dot{\psi}^2\sin\phi\cos\phi \ + I_e u\dot{\psi}\cos(\phi)) \\ &\quad + \mathbf{b}_2(J_2\ddot{\psi}\sin(\phi) + J_4\dot{\psi}^2\cos^2(\phi) - J_4\dot{\phi}^2 \ + (J_1 + J_2 - J_3)\dot{\psi}\dot{\phi}\cos(\phi) - I_e\dot{u}) \\ &\quad + \mathbf{b}_3(J_4\ddot{\phi} + J_3\ddot{\psi}\cos(\phi) - J_4\dot{\psi}^2\sin(\phi)\cos(\phi) \ + (J_2 - J_3 - J_1)\dot{\psi}\dot{\phi}\sin(\phi) - I_e u\dot{\phi}), \end{aligned} \tag{A.19}$$

where

$$I_e = \frac{I_{er}}{r_r + r_{rt}} + \frac{I_{ef}}{r_f + r_{ft}}. \tag{A.20}$$

Equating the above two expressions for $\mathbf{M}$ and isolating components gives three scalar equations that impose a balance of angular momentum on the motorcycle.

A.6.3 Tire Forces

Following Cossalter et al. [4], the lateral force $\mathbf{F}_r$ on the rear tire of the motorcycle evolves according to

$$\frac{\sigma_r}{u}\dot{F}_r + F_r = C_1\lambda + C_2\phi, \tag{A.21}$$

where σ_r is the tire relaxation length, C_1 and C_2 are constants, and $\lambda = \arctan(v/u)$ is the side-slip angle.

A.7 Reduction of the Equations

Setting r_{ft} and r_{rt} equal to the common radius r_t allows us to solve for $\ddot{\psi}$ and $\ddot{\phi}$:

$$\begin{bmatrix}\ddot{\psi}\\ \ddot{\phi}\end{bmatrix} = \begin{bmatrix}-A_{22} & A_{12}\\ -A_{21} & A_{11}\end{bmatrix}\begin{bmatrix}B_1\\ B_2\end{bmatrix}\frac{1}{A_{11}A_{22} - A_{12}A_{21}} \tag{A.22}$$

where

$$\begin{aligned}
A_{11} &= J_4\cos(\phi)\\
A_{22} &= J_4\cos(\phi)\\
A_{12} &= J_1 + mh\sin^2(\phi)(h - r_t)\\
A_{21} &= J_2\sin^2(\phi) + J_3\cos^2(\phi) - hI_e\sin^2(\phi)\\
B_1 &= -h(F_r + F_f)\cos(\phi) + m(g - h\dot{\phi}^2\cos(\phi))\sin(\phi)(h - r_t)\\
&\quad - (J_3 - J_2)\dot{\psi}^2\sin(\phi)\cos(\phi) - uI_e\dot{\psi}\cos(\phi)\\
B_2 &= (S_r + S_f - F_a)(r_t - h - \frac{I_e}{m})\sin\phi + F_r b - F_f(p - b)\\
&\quad + (J_2 - J_3)2\dot{\psi}\dot{\phi}\sin\phi\cos\phi + J_4\dot{\phi}^2\sin(\phi) - uI_e\dot{\phi}\cos(\phi)\\
&\quad - I_e\sin(\phi)(+v\dot{\psi} + b\dot{\psi}^2 + 2h\dot{\psi}\dot{\phi}\cos(\phi)) - M_f - M_r
\end{aligned} \tag{A.23}$$

A.8 Differences with Cossalter et al.

The preceding model is based on a set of equations given by Cossalter et al. [4]. In particular, the derivation given in this appendix is original. Correspondence between O'Reilly and Cossalter revealed that Cossalter's equations were obtained with the aid of a software package. A close comparison of Cossalter's equations and ours reveals only minor differences, which are attributable to different assumptions on the road contact geometry of the motorcycle tires. Also, our equations include vertical moments acting on the motorcycle wheels as a result of their contact with the ground.

B Background Dynamics

B.1 Balance of Angular Momentum With Respect to an Arbitrary Point

In this section we establish some results pertaining to the dynamics of rigid bodies. Let B be a rigid body, let *the origin* locate a fixed point in space, and let $\mathbf{x}_A$ locate an arbitrary point in space. The moment $\mathbf{M}_0$ on B about the origin caused by a set of forces $\{\mathbf{f}_i\}$ acting on the body is given by

$$\mathbf{M}_0 = \sum \mathbf{x}_i \times \mathbf{f}_i, \tag{B.1}$$

where $\mathbf{x}_i$ locates the point on ∂B where $\mathbf{f}_i$ is applied. The moment $\mathbf{M}_A$ on B about $\mathbf{x}_A$ due to $\{\mathbf{f}_i\}$ is given by

$$\begin{aligned} \mathbf{M}_A &= \sum (\mathbf{x}_i - \mathbf{x}_A) \times \mathbf{f}_i \\ &= \mathbf{M}_0 - \mathbf{x}_A \times \sum \mathbf{f}_i. \end{aligned} \tag{B.2}$$

The angular momentum $\mathbf{H}_0$ of B about the origin is defined by

$$\mathbf{H}_0 = \int_B (\mathbf{x} \times \dot{\mathbf{x}}) \rho dv, \tag{B.3}$$

and the angular momentum $\mathbf{H}_A$ of B about $\mathbf{x}_A$ is defined by

$$\begin{aligned} \mathbf{H}_A &= \int_B ((\mathbf{x} - \mathbf{x}_A) \times \dot{\mathbf{x}}) \rho dv \\ &= \mathbf{H}_0 - \mathbf{x}_A \times \mathbf{G}, \end{aligned} \tag{B.4}$$

where $\mathbf{G} = m\dot{\mathbf{x}}$ with m equal to the mass of B. When $\mathbf{x}_A$ equals the center of mass $\tilde{\mathbf{x}}$ of B_i, $\mathbf{H}_A$ becomes the angular momentum of B_i about its center of mass, and is denoted $\mathbf{H}$ giving

$$\mathbf{H} = \mathbf{H}_0 - \tilde{\mathbf{x}} \times \mathbf{G}. \tag{B.5}$$

Using the Euler postulate $\mathbf{M}_0 = \dot{\mathbf{H}}_0$ to combine (B.2) and (B.4), and using $\sum \mathbf{f}_i = \dot{\mathbf{G}}$ (the other Euler postulate) to eliminate terms from the resulting expression, we find that

$$\mathbf{M}_A = \dot{\mathbf{H}}_A + \dot{\mathbf{x}}_A \times \mathbf{G}. \tag{B.6}$$

We note that when $\mathbf{x}_A$ is the center of mass of B, $\mathbf{G} = m\dot{\mathbf{x}}_A$ and so $\dot{\mathbf{x}}_A \times \mathbf{G} = \mathbf{0}$, leaving us with $\mathbf{M} = \dot{\mathbf{H}}$ where $\mathbf{H}$ has been introduced as our notation for the angular momentum of B about its center of mass, and where we let $\mathbf{M}$ denote the moment on B about its center of mass.

B.2 A Collection of Constrained Rigid Bodies

We now concern ourselves with a collection of n rigid bodies, each denoted B_i, constrained so that their centers of mass are fixed distances from each other. The angular momentum balance (B.6) for each B_i is given by

$$\sum \mathbf{M}_{Ai} = \dot{\mathbf{H}}_{Ai} + \dot{\mathbf{x}}_{Ai} \times \mathbf{G}_i, \tag{B.7}$$

where the point $\mathbf{x}_A$ has been chosen to be the center of mass of the collection. We now sum the momentum balance equations (B.7) for all B_i's. The fact that $\mathbf{x}_A$ is the same in every balance equation (B.7) relieves us of having to consider moments acting on the bodies which arise because of constraints. (Such moments acting on one body will necessarily act on another body in an equal and opposite manner). Letting $\mathbf{M}$ denote the net external moment acting on the collection of bodies with respect to $\mathbf{x}_A$, this summation takes the form

$$\mathbf{M} = \frac{d}{dt}\left(\mathbf{H}_{A1} + \cdots + \mathbf{H}_{An}\right) + \dot{\mathbf{x}}_A \times \left(\mathbf{G}_1 + \cdots + \mathbf{G}_n\right). \tag{B.8}$$

The term above involving the summation of $\mathbf{G}_i$'s vanishes because this sum equals the total mass of all the bodies multiplied by $\dot{\mathbf{x}}_A$. Letting $\boldsymbol{\pi}_i = \tilde{\mathbf{x}}_i - \mathbf{x}_A$, we use (B.4) and (B.5) to express the summation of $\mathbf{H}_{Ai}$'s in (B.8) as

$$\sum \mathbf{H}_{Ai} = \sum \mathbf{H}_i + \sum \boldsymbol{\pi}_i \times \mathbf{G}_i. \tag{B.9}$$

It is a fundamental result in mechanics that $\mathbf{H}_i = \mathbf{J}_i \boldsymbol{\omega}_i$ where $\mathbf{J}_i$ is the inertia tensor of B_i about its center of mass, and where $\boldsymbol{\omega}_i$ is the angular velocity of B_i. The derivation of this result is similar to the development we give now of the summation of $\boldsymbol{\pi}_i \times \mathbf{G}_i$ terms in (B.9). Because the centers of masses of all the bodies B_i are fixed distances from each other, we have $\dot{\boldsymbol{\pi}}_i = \tilde{\boldsymbol{\omega}} \times \boldsymbol{\pi}_i$, where $\tilde{\boldsymbol{\omega}}$ is the angular velocity of the collection of rigid body mass centers, and

$$\begin{aligned}
\sum \boldsymbol{\pi}_i \times \mathbf{G}_i &= \sum \boldsymbol{\pi}_i \times (\tilde{\boldsymbol{\omega}} \times \boldsymbol{\pi}_i) m_i \\
&= \sum \left(\tilde{\boldsymbol{\omega}} (\boldsymbol{\pi}_i \cdot \boldsymbol{\pi}_i) \ - \boldsymbol{\pi}_i (\tilde{\boldsymbol{\omega}} \cdot \boldsymbol{\pi}_i) \right) m_i \\
&= \left[\sum m_i \left(\mathbf{I} (\boldsymbol{\pi}_i \cdot \boldsymbol{\pi}_i) \ - \boldsymbol{\pi}_i \otimes \boldsymbol{\pi}_i \right) \right] \tilde{\boldsymbol{\omega}} \\
&= \tilde{\mathbf{J}} \tilde{\boldsymbol{\omega}},
\end{aligned} \tag{B.10}$$

where the newly defined tensor $\tilde{\mathbf{J}}$ is to a collection of point masses m_i at points $\tilde{\mathbf{x}}_i$ of a rigid spatial lattice what $\mathbf{J}_i$ is to the mass in the rigid body B_i. Compiling our results, (B.8) becomes

$$\mathbf{M} = \frac{d}{dt}(\tilde{\mathbf{J}} \tilde{\boldsymbol{\omega}}) + \sum \frac{d}{dt}(\mathbf{J}_i \boldsymbol{\omega}_i). \tag{B.11}$$

C Simple Models

C.1 An Inverted Point Mass Pendulum

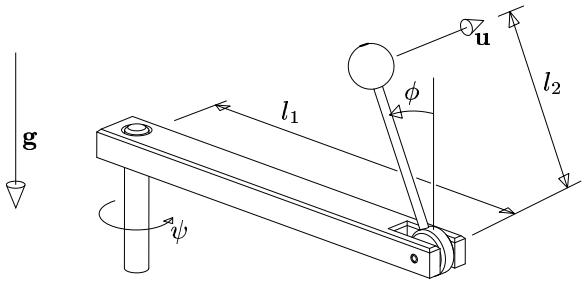

Figure 21: Schematic of the inverted pendulum motorcycle model.

Our interest is in the time evolution of ϕ in the system shown above. The horizontal beam of length l_1 is spun about the vertical at the rate $\dot{\psi}(t)$. The rod of length l_2 is pivoted to this beam and rotates through the angle ϕ. The point mass (shown as a sphere) at the end of this rod is subject to constraint forces and to a downward acting gravitational force. It can be shown that the parameter ϕ evolves according to

$$\ddot{\phi} = \frac{g \sin\phi}{l_2} - \dot{\psi}^2 \frac{l_1 - l_2 \sin\phi}{l_2} \cos\phi. \tag{C.1}$$

We now consider the special equilibrium case, in which $\dot{\phi} = 0$. This condition causes (C.1) to reduce to

$$\sin\phi = \frac{L\dot{\psi}^2}{g} \cos\phi, \tag{C.2}$$

where $L = l_1 - l_2 \sin\phi$. The point mass velocity $\mathbf{u}$ under the equilibrium condition is depicted in the diagram above. Noting that the magnitude u of this vector is given by $u = L\dot{\psi}$, and that the value ω that would be measured by a gyroscope aligned with the rod axis is given by $\omega = \dot{\psi}\cos\phi$, we can rewrite (C.2) as

$$\sin\phi = \frac{u\omega}{g}. \tag{C.3}$$

We note that the equilibrium values of ϕ that interest us are unstable. Hence, although (C.3) may offer a reasonable prediction of motorcycle roll, it cannot be used to predict variation in ϕ about the equilibrium value (unless perhaps we add a controller that mimics the efforts of the motorcyclist to keep the motorcycle tilted at the proper angle).

C.2 An Inverted Rectangular Slab

Here we model the motorcycle not as a point mass but as a rigid plate, as shown in Figure 22. A balance of angular momentum of the plate reads as

$$\sum \mathbf{M}_y = \dot{\mathbf{H}}_x + (\mathbf{x} - \mathbf{y}) \times m\ddot{\mathbf{x}}, \tag{C.4}$$

where m is the total mass of the plate. Each of the terms in this expression is straightforward to develop. Assuming $\dot{\psi}$ and ϕ are both constant (i.e., that an equilibrium value of ϕ has been found corresponding to the unchanging value of $\dot{\psi}$, the plate angular velocity is given by $\boldsymbol{\omega} = \dot{\psi}\mathbf{e}_3$. The plate angular momentum $\mathbf{H}_x$ about its center of mass is given by $\mathbf{J}\boldsymbol{\omega}$ where the components of the inertia tensor $\mathbf{J}$ are given with respect to the $\{\mathbf{e}_i \otimes \mathbf{e}_j\}$ basis by

$$[\mathbf{J}] = \begin{bmatrix} \cos\phi & 0 & \sin\phi \\ 0 & 1 & 0 \\ -\sin\phi & 0 & \cos\phi \end{bmatrix} \begin{bmatrix} \lambda_1 & 0 & 0 \\ 0 & \lambda_2 & 0 \\ 0 & 0 & \lambda_3 \end{bmatrix} \begin{bmatrix} \cos\phi & 0 & -\sin\phi \\ 0 & 1 & 0 \\ \sin\phi & 0 & \cos\phi \end{bmatrix}. \tag{C.5}$$

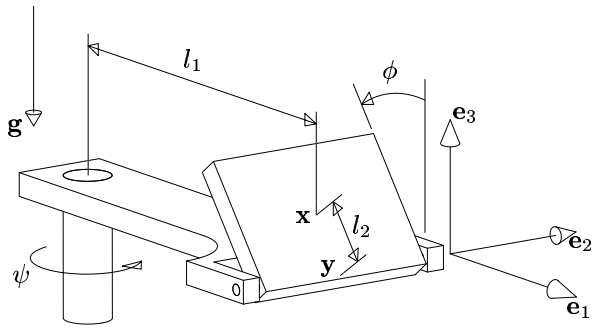

Figure 22: Schematic of the inverted plate motorcycle model. The plate is pivoted to a beam that rotates about the vertical. The basis $\{\mathbf{e}_i\}$ is fixed to this beam. The plate center of mass is given by $\mathbf{x}$, and the intersection of the plate pivot axis with the plane spanned by $\{\mathbf{e}_1, \mathbf{e}_3\}$ that also contains $\mathbf{x}$ is given by $\mathbf{y}$. Note that $\mathbf{x}$ and $\mathbf{y}$ are both material points within the plate.

Differentiating $\mathbf{H}_x$, (and noting that $\dot{\boldsymbol{\omega}} = \mathbf{0}$), we find that

$$\dot{\mathbf{H}}_x = \boldsymbol{\omega} \times \mathbf{J}\boldsymbol{\omega} = \dot{\psi}^2(\lambda_3 - \lambda_1)\sin\phi\cos\phi\mathbf{e}_2. \tag{C.6}$$

Next, we note that

$$(\mathbf{x} - \mathbf{y}) \times m\ddot{\mathbf{x}} = -m\dot{\psi}^2 l_1 l_2 \cos\phi\mathbf{e}_2. \tag{C.7}$$

Substituting (C.6) and (C.7) into (C.4), and denoting $\omega = \dot{\psi}\cos\phi$ and $u = \dot{\psi}l_2$, we find that

$$\sin\phi = \frac{u\omega}{g} + \omega^2\frac{\lambda_1 - \lambda_3}{mgl}\tan\phi. \tag{C.8}$$

C.3 Avery's Minor Radius Accommodation

We now consider a model that accounts for the minor radius of the (approximately toroidal) tires of a motorcycle. This model was suggested by Avery Jutkowitz and is shown in Figure 23. For this model a

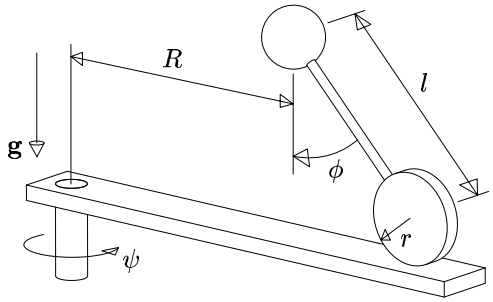

Figure 23: Schematic of Avery's motorcycle model. This model is exactly like the inverted point mass pendulum model except that instead of pivoting about a definite axis, the inverted pendulum engages the horizontal beam through the disk of radius r, which rolls without slipping. The disk is constrained not to tilt side to side, or to roll in anything other than a straight line in the direction of the beam axis of rotation. We let R_0 denote the value the dimension R would have if ϕ were to equal 0.

Lagrangian derivation of the dynamics is easiest. With $\dot{\psi}$ constant and with $\dot{\phi} = 0$, the kinetic energy T and potential energy U associated with the point mass m are given by

$$\begin{aligned} T &= \frac{1}{2}m(\dot{\psi}(R_0 - r\phi - l\sin\phi))^2 \\ U &= mgl\cos\phi \end{aligned} \tag{C.9}$$

Setting $L = T - U$ and recalling that for this system, $\frac{d}{dt}\left(\frac{\partial L}{\partial \dot{\phi}}\right) - \frac{\partial L}{\partial \phi} = 0$, we immediately find that

$$\sin\phi = \frac{u\omega}{g}(1 + \frac{r}{l\cos\phi}) \tag{C.10}$$

where we have introduced $\omega = \dot{\psi}\cos\phi$. We note that as $r \longrightarrow 0$, (C.10) approaches (C.3) as expected.

D Inertial Sensor Signal Processing

In this Appendix, we address tracking the motorcycle using traditional methods of inertial navigation. In theory, given three gyroscopes and three accelerometers, it is possible to determine the orientation and position of an object moving in the presence of a gravitational field. First, data from the gyroscopes is integrated to provide the object's orientation. Then, given the gravitational force acting on the object (which is generally a function of the object's position), as well as data from the accelerometers, it is possible to determine the object's acceleration. Integration of the acceleration yields velocity and position.

When the moving object in question is a motorcycle being driven over a (flat) road, the fact that velocity usually occurs in the forward direction of the motorcycle makes it advantageous to work with a basis $\{\mathbf{a}_i\}$ that is aligned with the motorcycle frame, rather than with respect to one which is immobile. Size and cost considerations for a motorcycle mounted system cause us to use the "strap-down" approach, in which gyroscopes and accelerometers are fixed rigidly to the object being observed. Also, because we intend to use INS as an interpolation device during the brief time intervals between GPS and map matching corrections, considerations such as the curvature and rotation of the Earth, and variation in the Earth's gravitational field will not concern us. We may think of motion as occurring over a flat inertial plane, perpendicular to a constant downward pointing gravity vector. Although we eventually intend to account for variability in terrain, our present analysis is restricted to the simplified case of motion over a perfectly flat level surface.

D.1 Preliminaries

Different bases are involved in our analysis and it is helpful to work out the relationships between them ahead of time[6]. The output axes of the sensor are presumed to be aligned with the orthonormal "platform fixed" basis $\{\mathbf{e}_i\}$, which we note is also body fixed because the sensors are "strapped down" to the frame of the motorcycle. An inertial basis $\{\mathbf{E}_i\}$ is chosen so that the acceleration due to gravity is given by $\mathbf{g} = g\mathbf{E}_3$ (the local ground tangent plane is treated as inertial and $\mathbf{E}_3$ is in the downward direction). The orientation of $\{\mathbf{e}_i\}$ with respect to $\{\mathbf{E}_i\}$ can be parameterized by a 3-1-2 sequence of Euler angle rotations. First, we rotate the basis $\{\mathbf{E}_i\}$ through a "yaw" angle ψ about the $\mathbf{E}_3$ axis, generating the new basis $\{\mathbf{a}_i\}$:

$$\begin{bmatrix}\mathbf{a}_1\\ \mathbf{a}_2\\ \mathbf{a}_3\end{bmatrix} = \begin{bmatrix}\cos\psi & \sin\psi & 0\\ -\sin\psi & \cos\psi & 0\\ 0 & 0 & 1\end{bmatrix}\begin{bmatrix}\mathbf{E}_1\\ \mathbf{E}_2\\ \mathbf{E}_3\end{bmatrix}. \tag{D.1}$$

Next, we rotate the basis $\{\mathbf{a}_i\}$ through a "roll" angle ϕ about the $\mathbf{a}_1$ axis, generating the new basis $\{\mathbf{b}_i\}$:

$$\begin{bmatrix}\mathbf{b}_1\\ \mathbf{b}_2\\ \mathbf{b}_3\end{bmatrix} = \begin{bmatrix}1 & 0 & 0\\ 0 & \cos\phi & \sin\phi\\ 0 & -\sin\phi & \cos\phi\end{bmatrix}\begin{bmatrix}\mathbf{a}_1\\ \mathbf{a}_2\\ \mathbf{a}_3\end{bmatrix}. \tag{D.2}$$

Finally, we rotate the basis $\{\mathbf{b}_i\}$ through a "pitch" angle θ about the $\mathbf{b}_2$ axis, generating the $\{\mathbf{e}_i\}$ basis:

$$\begin{bmatrix}\mathbf{e}_1\\ \mathbf{e}_2\\ \mathbf{e}_3\end{bmatrix} = \begin{bmatrix}\cos\theta & 0 & -\sin\theta\\ 0 & 1 & 0\\ \sin\theta & 0 & \cos\theta\end{bmatrix}\begin{bmatrix}\mathbf{b}_1\\ \mathbf{b}_2\\ \mathbf{b}_3\end{bmatrix}. \tag{D.3}$$

Combining the three equations above, we find that

$$\begin{bmatrix}\mathbf{e}_1\\ \mathbf{e}_2\\ \mathbf{e}_3\end{bmatrix} = \begin{bmatrix}(\cos\psi\cos\theta - \sin\psi\sin\phi\sin\theta) & (\sin\psi\cos\theta + \cos\psi\sin\phi\sin\theta) & -\cos\phi\sin\theta\\ -\sin\psi\cos\phi & \cos\psi\cos\phi & \sin\phi\\ (\cos\psi\sin\theta + \sin\psi\sin\phi\cos\theta) & (\sin\phi\sin\theta - \cos\phi\sin\phi\cos\theta) & \cos\phi\cos\theta\end{bmatrix}\begin{bmatrix}\mathbf{E}_1\\ \mathbf{E}_2\\ \mathbf{E}_3\end{bmatrix}. \tag{D.4}$$

[6] All the bases and Euler angles used in Appendix A are used again here, with their relationship to the motorcycle maintained. A diagram of these bases and angles is given in Figure 20.

D.2 Gyroscope Output

A standard result [13] allows us to write the angular velocity $\boldsymbol{\omega}$ of the sensor array as

$$\boldsymbol{\omega} = \dot{\psi}\mathbf{E}_3 + \dot{\phi}\mathbf{a}_1 + \dot{\theta}\mathbf{e}_2. \tag{D.5}$$

Using (D.3) and (D.4) and writing $\boldsymbol{\omega} = \omega_i \mathbf{e}_i$, we find that

$$\begin{bmatrix}\omega_1\\ \omega_2\\ \omega_3\end{bmatrix} = \begin{bmatrix}-\cos\phi\sin\theta & \cos\theta & 0\\ \sin\phi & 0 & 1\\ \cos\phi\cos\theta & \sin\theta & 0\end{bmatrix}\begin{bmatrix}\dot{\psi}\\ \dot{\phi}\\ \dot{\theta}\end{bmatrix}, \tag{D.6}$$

and inversely that

$$\begin{bmatrix}\dot{\psi}\\ \dot{\phi}\\ \dot{\theta}\end{bmatrix} = \begin{bmatrix}-\sec\phi\sin\theta & 0 & \sec\phi\cos\theta\\ \cos\theta & 0 & \sin\theta\\ \tan\phi\sin\theta & 1 & -\tan\phi\cos\theta\end{bmatrix}\begin{bmatrix}\omega_1\\ \omega_2\\ \omega_3\end{bmatrix}. \tag{D.7}$$

Equation (D.7) will be referred to later on in the abbreviated form $\dot{\lambda}_i = E_{ij}\omega_j$. We assume that the gyroscope portion of the sensor outputs the signals ω_i. Knowing the Euler angles ψ_0, ϕ_0, and θ_0 at an initial time t_0, and $\omega_i(t)$ at every time $t \geq t_0$, we can integrate (D.7) to determine $\psi(t)$, $\phi(t)$, and $\theta(t)$. These angles parameterize the sensor array's orientation.

D.3 Accelerometer Output

The accelerometer can be thought of as consisting of a test mass m suspended in an enclosure by a system of springs of stiffness k, and dampers with dissipative constants c. (Actually, the accelerometer probably consists of three one dimensional spring mass damper systems in an orthogonal array, however thinking of the accelerometer as a single mass suspended in space streamlines our discussion). Let $\mathbf{x}$ be the position

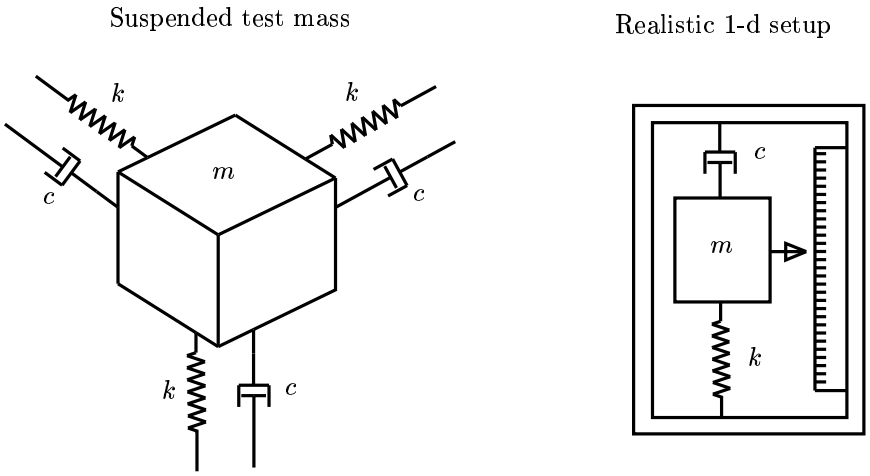

Figure 24: Test mass suspended by springs and dampers.

vector of the center of the enclosure (where the mass would be at equilibrium), relative to an inertial frame of reference. Let $\mathbf{s}$ be the displacement vector of the mass m from its equilibrium position (so the position vector of the mass is given by $\mathbf{x} + \mathbf{s}$. The forces acting on m are a gravitational body force $m\mathbf{g}$, a restoring force $-k\mathbf{s}$ due to the springs, and a dissipative force $-c\dot{\mathbf{s}}$ due to the dampers. Balancing forces, we find that the absolute acceleration vector $(\ddot{\mathbf{x}} + \ddot{\mathbf{s}})$ of the mass m satisfies

$$m\mathbf{g} - k\mathbf{s} - c\dot{\mathbf{s}} = m(\ddot{\mathbf{x}} + \ddot{\mathbf{s}}). \tag{D.8}$$

The forcing term $m(\mathbf{g} - \ddot{\mathbf{x}})$ can be viewed as exciting the displacement vector $\mathbf{s}$.

$$m\ddot{\mathbf{s}} + c\dot{\mathbf{s}} + k\mathbf{s} = m(\mathbf{g} - \ddot{\mathbf{x}}). \tag{D.9}$$

Assuming that transients in $\mathbf{s}$ die off on a time scale which is much smaller than that of the forcing, $\mathbf{s}$ quickly reaches a steady value given by

$$\mathbf{s} = \frac{m}{k}(\mathbf{g} - \ddot{\mathbf{x}}). \tag{D.10}$$

The signals $s_i = \frac{k}{m}\mathbf{s} \cdot \mathbf{e}_i$ comprise the accelerometer output. Notice that we scale the output by the factor k/m so that it is in units of g. Our interest is in using these signals to find the velocity $\dot{\mathbf{x}}$ of the sensor. As mentioned initially, it is to our advantage to work with respect to the basis $\{\mathbf{a}_i\}$. To this end, we define $q_i = \frac{k}{m}\mathbf{s} \cdot \mathbf{a}_i$, which, from (D.2) and (D.3), we can see are related to the accelerometer signals s_i by

$$\begin{bmatrix} q_1 \\ q_2 \\ q_3 \end{bmatrix} = \begin{bmatrix} \cos\theta & 0 & \sin\theta \\ \sin\phi\sin\theta & \cos\phi & -\sin\phi\cos\theta \\ -\cos\phi\sin\theta & \sin\phi & \cos\phi\cos\theta \end{bmatrix} \begin{bmatrix} s_1 \\ s_2 \\ s_3 \end{bmatrix}. \tag{D.11}$$

This equation will be refered to later on in the abbreviated form $q_i = F_{ij}s_j$. We know that $\mathbf{g} = g\mathbf{E}_3 = g\mathbf{a}_3$, so it only remains to resolve $\ddot{\mathbf{x}}$ against the $\{\mathbf{a}_i\}$ basis. If $\dot{\mathbf{x}}$ is written as $v_i\mathbf{a}_i$, then $\ddot{\mathbf{x}} = \dot{v}_i\mathbf{a}_i + v_i\dot{\mathbf{a}}_i$, where $\dot{\mathbf{a}}_1 = \dot{\psi}\mathbf{a}_2$, $\dot{\mathbf{a}}_2 = -\dot{\psi}\mathbf{a}_1$, and $\dot{\mathbf{a}}_3 = \mathbf{0}$. It now follows from (D.10) that

$$\begin{aligned} \dot{v}_1 &= -q_1 + \dot{\psi}v_2, \\ \dot{v}_2 &= -q_2 - \dot{\psi}v_1, \\ \dot{v}_3 &= -q_3 + g. \end{aligned} \tag{D.12}$$

Integrating the signals $\dot{v}_i$ gives us the components v_i of the velocity vector of the sensor with respect to the basis $\{\mathbf{a}_i\}$. Because these are the velocity components of a motorcycle traveling over a (flat) road, we expect that only the forward component v_1 will be nonzero. If desired, subsequent integration given v_1 and ψ will give the motorcycle position. A full schematic of the process we use is given below:

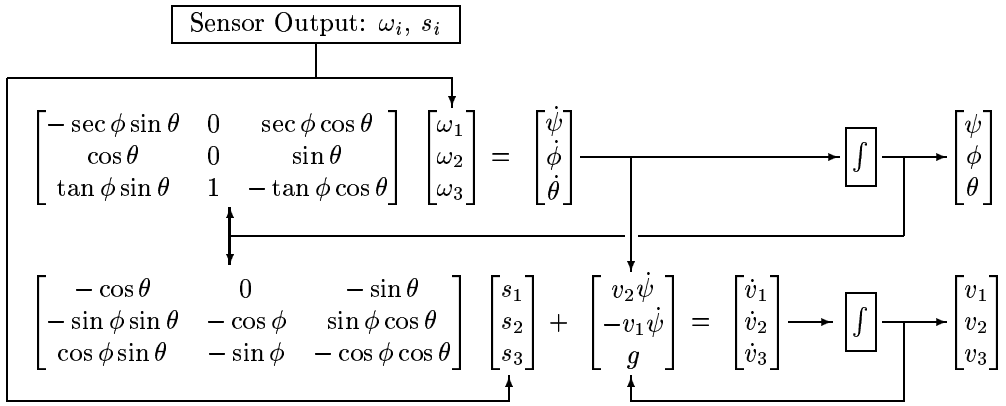

Flowchart C.1: The Complete Algorithm.

D.4 Error Analysis

The formulae we have developed apply to actual parameter values x. In practice, the signals we manipulate never stay equal to the actual parameter values. To reflect this, we decompose actual parameter values x according to

$$x = \hat{x} + \delta x, \tag{D.13}$$

where $\hat{x}$ is a prediction of what the parameter value is. The error term δx is given by $x - \hat{x}$, where x and $\hat{x}$ are both well defined. The δx term includes for instance the effects of signal noise, sensor error, and calculation

error[7]. Suppose we are given

$$y = f(x), \tag{D.14}$$

which maps an actual parameter x to an actual parameter y. Replacing x with $\hat{x} + \delta x$ and expanding about $\hat{x}$ results in a decomposition of the right hand side of (D.14) into a part that contains no δx terms (given by $\hat{y} = f(\hat{x})$), and a part that does, (given by $\delta y = f(x) - f(\hat{x})$[8]. Hence given (D.14), the decomposition (D.13) of x results in a decomposition of y that is also in the form (D.13). If the error terms δx are sufficiently small, then we may safely neglect all terms of δy that are higher than first order in δx. (This greatly facilitates dealing with this part of the expansion). The expression for δy in terms of x and δx shows us the effect (D.14) has on input error. If (D.14) is a differential equation, then the expression for δy will be a differential equation for the error terms δy of the output of (D.14), and we will be able to track the time evolution of δy. Note that our decomposition is easily extended to the case of vector signals and nonlinear mappings of vector fields.

The time growth rate of error in a predicted signal $\hat{y}$ will increase with the number of successive time integrations involved in the calculation of the signal. The most desirable type of error term is that which does not grow with time, (i.e. that which is $O(t^0)$). We will often refer to signals with such error terms as primary signals.

D.4.1 Gyroscope

The gyroscope axes are aligned with a triad $\{\mathbf{h}_i\}$ of unit vectors. Although ideally $\{\mathbf{h}_i\}$ would coincide with the frame-fixed orthonormal basis $\{\mathbf{e}_i\}$, in practice a misalignment will exist, which we give by $\mathbf{e}_i = B_{ij}\mathbf{h}_j$. This misalignment is time invariant, and accommodates $\{\mathbf{h}_i\}$ that are not orthonormal. If an attempt is made to obtain the components B_{ij} experimentally, the values determined will be given by $\hat{B}_{ij} = B_{ij} - \delta B_{ij}$, where B_{ij} are actual values, and δB_{ij} are error terms. The gyroscope outputs are given by $\hat{\omega}_i = \omega_i^h - \delta\omega_i$ where $\omega_i^h = \boldsymbol{\omega}\cdot\mathbf{h}_i$, and where $\delta\omega_i$ is a time varying signal which accounts for error in the gyroscope mechanism and noise in its output. Recall that the Euler angles λ_i that parameterize the orientation of $\{\mathbf{e}_i\}$, evolve in time according to

$$\dot{\lambda}_i = E_{ij}\boldsymbol{\omega}\cdot\mathbf{e}_j = E_{ij}B_{jk}\omega_k^h, \tag{D.15}$$

where the E_{ij}'s are themselves functions of the Euler angles λ_i. Decomposing E_{ij} according to (D.13), we find that

$$\begin{aligned}\dot{\lambda}_i = E_{ij}B_{jk}\omega_k^h &= (\hat{E}_{ij} + \delta E_{ij})(\hat{B}_{jk} + \delta B_{jk})(\hat{\omega}_k + \delta\omega_k) \\ &= \hat{E}_{ij}\hat{B}_{jk}\hat{\omega}_k + \delta E_{ij}\hat{B}_{jk}\hat{\omega}_k + \hat{E}_{ij}\delta B_{jk}\hat{\omega}_k \ + \hat{E}_{ij}\hat{B}_{jk}\delta\omega_k + h.o.t.,\end{aligned} \tag{D.16}$$

where *h.o.t.* are *higher order terms*, which we neglect. It follows that the error $\delta\dot{\lambda}_i$ caused by our use of $\hat{E}_{ij}$, $\hat{B}_{ij}$, and $\hat{\omega}_i$ is given by

$$\delta\dot{\lambda}_i = \delta E_{ij}\hat{B}_{jk}\hat{\omega}_k + \hat{E}_{ij}\delta B_{jk}\hat{\omega}_k + \hat{E}_{ij}\hat{B}_{jk}\delta\omega_k. \tag{D.17}$$

This set of three coupled ordinary differential equations comprises an initial value problem for the three Euler angle errors $\delta\lambda_i(t)$. We note that $\hat{E}_{ij} = \hat{E}_{ij}(\hat{\phi}, \hat{\theta})$, so the error dynamics are affected by the system's trajectory[9].

[7] We note that different assignments of $\hat{x}$ result in different decompositons. Consider the roll ϕ of a motorcycle moving in a straight line. If we set $\hat{\phi}$ equal to its nominal value of 0, the error term $\delta\phi$ will make up for the fact that the actual motorcycle roll ϕ varies slightly about 0. If we try to measure the roll with a sensor, our signal $\hat{\phi}$ will not be constantly 0, and may actually be close to the actual motorcycle roll, however there will still be error $\delta\phi$, because no measurement is ever perfect.

[8] The value $\hat{y}$ is our prediction of the output, while δy is the difference between this prediction and the actual output.

[9] When B_{ij} is proper-orthogonal (in general it is not), and there are no sources of error besides sensor misalignment, error in $\lambda_i(t)$ can be eliminated by an appropriate choice of initial conditions $\{\psi_0, \phi_0, \theta_0\}$ in the integration of (D.7), (given by the Euler angles that parameterize B_{ij}).

D.4.2 Accelerometer

As with the gyroscope, the axes of the accelerometer are aligned with a triad $\{\mathbf{p}_i\}$ of unit vectors, which are assumed to differ from the basis $\{\mathbf{e}_i\}$ according to $\mathbf{e}_i = A_{ij}\mathbf{p}_j$, where the A_{ij}'s are time invariant and accommodate $\mathbf{p}_i$ that are not necessarily orthogonal. If determined experimentally, the components of this relation will be modeled by $\hat{A}_{ij} = A_{ij} - \delta A_{ij}$, where A_{ij} are actual values, and δA_{ij} are error terms[10]. The accelerometer output is given by $\hat{s}_i = s_i^p - \delta s_i$, where $s_i^p = (\mathbf{g} - \ddot{\mathbf{x}}) \cdot \mathbf{p}_i$, and where δs_i is a time varying signal which, like $\delta\omega_i$, accounts for error in the accelerometer mechanism as well as signal noise. Recall from (D.11) that $\mathbf{s} \cdot \mathbf{e}_i$ and q_i are related by

$$q_i = F_{ij}\mathbf{s} \cdot \mathbf{e}_j = F_{ij}A_{jk}s_k^p, \tag{D.18}$$

where the F_{ij}'s are functions of the Euler angles and therefore can be expanded to take the form $F_{ij} = \hat{F}_{ij} + \delta F_{ij}$. Combining F_{ij}, A_{jk}, and s_k^p, we find that

$$\begin{aligned} q_i = F_{ij}A_{jk}s_k^p &= (\hat{F}_{ij} + \delta F_{ij})(\hat{A}_{jk} + \delta A_{jk})(\hat{s}_k + \delta s_k) \\ &= \hat{F}_{ij}\hat{A}_{jk}\hat{s}_k + \delta F_{ij}\hat{A}_{jk}\hat{s}_k + \hat{F}_{ij}\delta A_{jk}\hat{s}^k \;\; + \hat{F}_{ij}\hat{A}_{jk}\delta s_k + h.o.t., \end{aligned} \tag{D.19}$$

where as before, *h.o.t.* are discarded. The error terms δq_i are consequently given by

$$\delta q_i = \delta F_{ij}\hat{A}_{jk}\hat{s}_k + \hat{F}_{ij}\delta A_{jk}\hat{s}_k + \hat{F}_{ij}\hat{A}_{jk}\delta s_k, \tag{D.20}$$

which when substituted into (D.12), result in the following error dynamics

$$\begin{aligned} \delta\dot{v}_1 &= -\delta q_1 + \hat{\dot{\psi}}\delta v_2 + \delta\dot{\psi}\hat{v}_2, \\ \delta\dot{v}_2 &= -\delta q_2 - \hat{\dot{\psi}}\delta v_1 - \delta\dot{\psi}\hat{v}_1, \\ \delta\dot{v}_3 &= -\delta q_3. \end{aligned} \tag{D.21}$$

D.4.3 An Expansion of δE_{ij} and δF_{ij}

Recall from (D.7) and (D.11) that E_{ij}, and F_{ij} are given by

$$\begin{aligned} [E_{ij}] &= \begin{bmatrix} -\sec\phi\sin\theta & 0 & \sec\phi\cos\theta \\ \cos\theta & 0 & \sin\theta \\ \tan\phi\sin\theta & 1 & -\tan\phi\cos\theta \end{bmatrix}, \\ [F_{ij}] &= \begin{bmatrix} \cos\theta & 0 & \sin\theta \\ \sin\phi\sin\theta & \cos\phi & -\sin\phi\cos\theta \\ -\cos\phi\sin\theta & \sin\phi & \cos\phi\cos\theta \end{bmatrix}. \end{aligned} \tag{D.22}$$

[10]The terms A_{ij} and B_{ij} characterize misalignment between the sensor axes and the basis $\{\mathbf{e}_i\}$. The nominal situation is that the accelerometer and gyroscope axes are perfectly aligned with the $\{\mathbf{e}_i\}$ basis, that is, $\hat{A}_{ij} = \delta_{ij}$ and $\hat{B}_{ij} = \delta_{ij}$. The terms δA_{ij} and δB_{ij} account for perturbations from this ideal. When misalignment is small, the off-diagonal terms of δA_{ij} and δB_{ij} will be small, and the diagonal terms will be much smaller, so much so that they can effectively be set to zero. When the misalignmnt consists of a rotation, δA_{ij} and δB_{ij} will be skew-symmetric.

Replacing λ_i with $\hat{\lambda}_i + \delta\lambda_i$, we find that to first order, δE_{ij} and δF_{ij} are given by

$$
\begin{aligned}
[\delta E_{ij}] =& \delta\phi \begin{bmatrix} -\tan\hat{\phi}\sec\hat{\phi}\sin\hat{\theta} & 0 & \tan\hat{\phi}\sec\hat{\phi}\cos\hat{\theta} \\ 0 & 0 & 0 \\ \tan\hat{\theta}\sec\hat{\theta} & 0 & -\sec\hat{\theta} \end{bmatrix} \\
&+\delta\theta \begin{bmatrix} -\sec\hat{\phi}\cos\hat{\theta} & 0 & -\sec\hat{\phi}\sin\hat{\theta} \\ -\sin\hat{\theta} & 0 & \cos\hat{\theta} \\ \tan\hat{\phi}\cos\hat{\theta} & 0 & \tan\hat{\phi}\sin\hat{\theta} \end{bmatrix}, \\
[\delta F_{ij}] =& \delta\hat{\phi} \begin{bmatrix} 0 & 0 & 0 \\ \cos\hat{\phi}\sin\hat{\theta} & -\sin\hat{\phi} & -\cos\hat{\phi}\cos\hat{\theta} \\ \sin\hat{\phi}\sin\hat{\theta} & \cos\hat{\phi} & -\sin\hat{\phi}\cos\hat{\theta} \end{bmatrix} \\
&+\delta\theta \begin{bmatrix} -\sin\hat{\theta} & 0 & \cos\hat{\theta} \\ \sin\hat{\phi}\cos\hat{\theta} & 0 & \sin\hat{\phi}\sin\hat{\theta} \\ -\cos\hat{\phi}\cos\hat{\theta} & 0 & -\cos\hat{\phi}\sin\hat{\theta} \end{bmatrix}.
\end{aligned} \tag{D.23}
$$

D.4.4 Motion of a Motorcycle

In the case of the motorcycle, $\hat{\theta}$, $\hat{v}_2$, and $\hat{v}_3$ are primary signals with nominal values of 0. Assuming perfect alignment of the gyroscope axes, we expand (D.17), and find that

$$
\begin{aligned}
\delta\dot{\psi} &= \delta\phi\hat{\omega}_3\tan\hat{\phi}\sec\hat{\phi} - \delta\theta\hat{\omega}_1\sec\hat{\phi} + \delta\omega_3\sec\hat{\phi}, \\
\delta\dot{\phi} &= \delta\theta\hat{\omega}_3 + \delta\omega_1, \\
\delta\dot{\theta} &= -\delta\phi\hat{\omega}_3 + \delta\theta\hat{\omega}_1\tan\hat{\phi} + \delta\omega_2 - \delta\omega_3\tan\hat{\phi}.
\end{aligned} \tag{D.24}
$$

The equation $(\text{D.24})_3$ for $\delta\dot{\theta}$ can be ignored because it only applies when $\hat{\theta}$ is calculated by a time integration involving the signals $\hat{\omega}_i$. In our case, $\hat{\theta}$ is a primary signal, and so $\delta\theta$ will be a small random signal with no structured growth in time. Assuming perfect alignment of the accelerometer axes, we expand (D.20) and (D.21), and find that

$$
\begin{aligned}
\delta\dot{v}_1 &= \hat{\dot{\psi}}\delta v_2 - \delta\theta\hat{s}_3 - \delta s_1, \\
\delta\dot{v}_2 &= -\hat{\dot{\psi}}\delta v_1 - \delta\dot{\psi}\hat{v}_1 \\
&\quad - \delta s_2\cos\hat{\phi} + \delta s_3\sin\hat{\phi} \\
&\quad + \delta\phi\hat{s}_2\sin\hat{\phi} + \delta\phi\hat{s}_3\cos\hat{\phi} - \delta\theta\hat{s}_1\sin\hat{\phi}, \\
\delta\dot{v}_3 &= -\delta s_2\sin\hat{\phi} - \delta s_3\cos\hat{\phi} \\
&\quad + \delta\theta\hat{s}_1\cos\hat{\phi} + \delta\phi\hat{s}_3\sin\hat{\phi} - \delta\phi\hat{s}_2\cos\hat{\phi}.
\end{aligned} \tag{D.25}
$$

As with $(\text{D.24})_3$, the formulae $(\text{D.25})_{2,3}$ for $\delta\dot{v}_2$ and $\delta\dot{v}_3$ can be ignored because $\hat{v}_2$ and $\hat{v}_3$ are both primary signals; we expect δv_2 and δv_3 to be small random signals with no structured growth in time.

D.4.5 Motorcycle Forward Velocity

We now use (D.24) and (D.25) to judge between two methods of calculating the forward velocity v_1 of the motorcycle. We wish to determine whether we would be better off using the accurate process from Flowchart C.1, or the approximate process given by

$$
\hat{v}_1(t) = \hat{v}_1(t_0) - \int_{t_0}^{t} \hat{s}_1(\tau)d\tau \tag{D.26}
$$

In using Flowchart C.1 we necessarily forgo the advantage had by treating $\hat{\theta}$, $\hat{v}_2$, and $\hat{v}_3$ as primary signals. Even though we know what these parameters will be, (for reasonable motorcycle motions they all have

nominal values of zero), we proceed to calculate them using Flowchart C.1, as if this information was not available[11]. With this in mind, the dynamics that govern the error terms for Flowchart C.1 reduce to the six equations in (D.24) and (D.25). The growth rates of the various error terms are easier to determine if we impose the additional restriction that the motorcycle move forward with constant velocity in a straight line[12]. For this motion, (D.24) reduces to

$$\delta\dot{\psi} = \delta\omega_3, \qquad \delta\dot{\phi} = \delta\omega_1, \qquad \delta\dot{\theta} = \delta\omega_2, \tag{D.27}$$

while (D.25) reduces to

$$\begin{aligned} \delta\dot{v}_1 &= -g\delta\theta - \delta s_1, \\ \delta\dot{v}_2 &= g\delta\phi - \delta s_2 - \hat{v}_1\delta\omega_3, \\ \delta\dot{v}_3 &= -\delta s_3. \end{aligned} \tag{D.28}$$

With the kinematics of turning and rolling out of the picture, it is easy to see that error in the Euler angles and in $\hat{v}_3$ is $O(t)$, while $\hat{v}_1$ and $\hat{v}_2$ both have error that is $O(t^2)$. We assume that these error growth rates also apply when the process in Flowchart C.1 is used to track general motorcycle motion over a plane (i.e., turning and rolling included). The reason for the $O(t^2)$ (i.e., poor) performance of the process in tracking v_1 is that the calculations for v_1 involve two time integrations in series. Although with perfect signals, the process would completely account for aberrant motorcycle motions (such as pitch and lateral slip during a turn), its performance is severely compromised by the growth characteristics of its error terms. In contrast, the error that arises as a result of the approximate process (D.26) is given by

$$\delta v_1 = \int_0^t (\hat{\dot{\psi}}\delta v_2 - \hat{s}_3\delta\theta - \delta s_1)dt, \tag{D.29}$$

where it can be calculated that

$$\hat{s}_3 = g\cos\hat{\phi} + \hat{v}_1\dot{\psi}\sin\hat{\phi} + l\hat{\dot{\phi}}^2 + l\hat{\dot{\psi}}^2\sin^2\hat{\phi}. \tag{D.30}$$

The parameter l is the distance from the ground to the location on the motorcycle frame of the accelerometer sensors when the motorcycle is upright. The important thing about (D.29) is that δv_2, $\delta\theta$, and δs_1 are all small with no time structure, because $\hat{\theta}$, $\hat{v}_2$, and $\hat{v}_3$ are treated as primary signals. This causes the error in (D.29) to be $O(t)$, which is much better than the $O(t^2)$ error resulting from the process shown in Flowchart C.1. The performance of (D.29) suffers when δv_2, $\delta\theta$, and δs_1 become excessively large, but δv_2 and $\delta\theta$ are small for reasonable motions of the motorcycle, and δs_1 is small when high enough quality sensors are used.

[11] The use of Flowchart C.1 would be warranted if we expected θ, v_2, and v_3 to have interesting non-zero values, and if we had sensors accurate enough to track these values over a reasonable length of time.

[12] Under these conditions, $\hat{v}_1$ is nonzero while $\hat{v}_2$ and $\hat{v}_3$ are both zero. The accelerometer signals are given by $\hat{s}_1 = 0$, $\hat{s}_2 = 0$, and $\hat{s}_3 = g$ and the gyroscope signals by $\hat{\omega}_i = 0$. We will suppose that the constant orientation of the sensor array is given by $\hat{\lambda}_i = 0$, (that is, each of the Euler angles is zero). We also assume that the gyroscope and accelerometer axes are perfectly aligned with the $\{\mathbf{e}_i\}$ basis.

E Algorithm Refinement

In this section we refine the basic navigation algorithm, and consider details that might arise if it is implemented in real time. We use the same motorcycle configurational parameters that we used in Appendix A, and once again we restrict our analysis to motorcycle motion over a horizontal plane. We assume that the available signals from the motorcycle are:

(i) ω_3: an effectively continuous angular velocity signal from a gyroscope mounted rigidly to the motorcycle frame (with sensing axis vertical when the motorcycle is upright).

(ii) t_i: a stream of discrete time values, each corresponding to a definite angular increment Φ in the rotational position of the rear wheel.

When a new time value t_i registers, it is known that the motorcycle rear wheel has undergone a rotation Φ. The corresponding increment in motorcycle distance (along its direction of travel) is given by $d = R\Phi$, where R is the momentary effective radius of the rear tire. This radius will depend on the roll angle ϕ in a way that we suggest can be modeled by the changing effective radius of a rigid torus rolling on a flat surface:

$$R = r_1 + r_2 \cos(\phi), \tag{E.1}$$

where r_1 and r_2 are respectively the major and minor radii of the torus. Using the notation $\Delta t_i = t_i - t_{i-1}$, the motorcycle speed at time t_i can be approximated as

$$v_i = R\Phi \left(\frac{1}{\Delta t_i} \right), \tag{E.2}$$

or, more accurately, as

$$v_i = R\Phi \left(\frac{2(\Delta t_{i-1})^2 + 2\Delta t_{i-1}\Delta t_i - (\Delta t_i)^2}{(\Delta t_{i-1} + \Delta t_i)\Delta t_{i-1}\Delta t_i} \right), \tag{E.3}$$

where the second formula requires that the two time values prior to t_i be available. The speed value v_i is that of the contact point between the rear wheel and the ground. We assume that the wheel rolls without slipping, and does not slide transverse to the direction the motorcycle is pointing, so that v_i completely specifies the velocity of this point. The direction the motorcycle is pointing is given by the yaw angle ψ. If this is known, then the Cartesian coordinates of the rear wheel contact point's position are given by

$$x = \sum R\Phi \cos\psi, \qquad y = \sum R\Phi \sin\psi. \tag{E.4}$$

Because we are restricting our analysis to the motion of a motorcycle over a flat plane, the Euler angle θ has a nominal value of 0. Although factors such as motorcycle acceleration and potholes will move θ away from 0, we generally expect $\delta\theta$ to be small with no structured growth in time. We also assume that the motorcycle roll ϕ can be well approximated as a function of the motorcycle speed v and the gyroscope signal ω_3 so that $\delta\phi$ is consistently small with no structured growth in time. Several formulae for $\phi(v, \omega_3)$ are discussed in Appendix C of this work. The remaining Euler angle ψ must be found using (D.7), which gives the general relationship between Euler angle rates $\dot{\lambda}_i$ and angular velocity components ω_i. The only part of this relationship of interest to us is the expression for $\dot{\psi}$, which, because of the zero nominal value of θ simplifies to

$$\dot{\psi} = \omega_3 \sec\phi. \tag{E.5}$$

This signal can be integrated to give the motorcycle yaw angle ψ. An overview of our navigation scheme is given below:

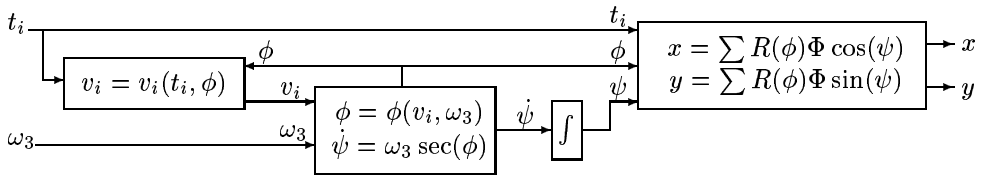

E.1 Error Analysis

A discussion of our method of error analysis is provided in Appendix D.4. In brief, every actual signal x is replaced by the sum of a predicted signal $\hat{x}$ and an error term δx. The decomposition of x results in a decomposition of every function of x into a function of $\hat{x}$ and a function of $\hat{x}$ and δx. This second function shows how error δx moves through our calculations. The expression $(D.24)_1$ for $\delta\dot{\psi}$ from Appendix D applies directly to our current navigation system.

$$\begin{aligned}\delta\dot{\psi} &= \delta\phi\hat{\omega}_3 \tan\hat{\phi}\sec\hat{\phi} - \delta\theta\hat{\omega}_1 \sec\hat{\phi} \ + \delta\omega_3 \sec\hat{\phi} \\ &= \sec\hat{\phi}(\delta\phi\dot{\hat{\psi}} - \delta\theta\dot{\hat{\phi}} + \delta\omega_3). \end{aligned} \tag{E.6}$$

As was noted earlier, the increment in motorcycle distance is given by $d = R\Phi$. Although Φ is known very precisely, it is reasonable to expect error in our prediction of R. The radius R is a function of r_1, r_2, and ϕ, each of which may be decomposed according to (D.13). Thus we have

$$r_1 = \hat{r}_1 + \delta r_1, \qquad r_2 = \hat{r}_2 + \delta r_2, \qquad \phi = \hat{\phi} + \delta\phi. \tag{E.7}$$

We expect to have to consider δr_1 and δr_2 because of variation in tire temperature and pressure, as well as because of tire wear. Expanding our expression d for the increment in motorcycle distance, and keeping only first order terms, we find that

$$d = \Phi(\hat{r}_1 + \hat{r}_2\cos\hat{\phi}) + \delta d, \tag{E.8}$$

where

$$\delta d = \Phi(\delta r_1 + \delta r_2\cos\hat{\phi} - \delta\phi\hat{r}_2\sin\delta\phi). \tag{E.9}$$

The output of our navigation scheme is the position of the motorcycle in Cartesian coordinates (E.4). When expanded according to (D.13), these expressions take the form

$$x = \sum \hat{s}\cos\hat{\psi} + \delta x, \qquad y = \sum \hat{s}\sin\hat{\psi} + \delta y, \tag{E.10}$$

where

$$\begin{aligned}\delta x &= \sum \Big(\Phi(\delta r_1 + \delta r_2\cos\hat{\phi} - \delta\phi\hat{r}_2\sin\hat{\phi})\cos\hat{\psi} \ - \Phi(\hat{r}_1 + \hat{r}_2\cos\hat{\phi})\delta\psi\sin\hat{\psi}\Big), \\ \delta y &= \sum \Big(\Phi(\delta r_1 + \delta r_2\cos\hat{\phi} - \delta\phi\hat{r}_2\sin\hat{\phi})\sin\hat{\psi} \ - \Phi(\hat{r}_1 + \hat{r}_2\cos\hat{\phi})\delta\psi\cos\hat{\psi}\Big). \end{aligned} \tag{E.11}$$

As mentioned previously, we assume that $\delta\phi$ is consistently small with no structured growth in time. The function $\hat{\phi} = \hat{\phi}(v, \omega_3)$ *does* differ from the actual roll of the motorcycle, but we have no way of studying this difference because we don't know what the actual roll of the motorcycle is. For the purpose of this analysis, we assume merely that the difference is small. The resultant treatment of ϕ as a primary signal relieves us of having to study the propagation through $\hat{\phi}(v, \omega_3)$ of error in v and ω_3, and indeed relieves us of having to study the error in v at all, because v isn't used for anything besides the prediction of ϕ. In the special case where $\hat{\phi}(v, \omega_3)$ is given by $\sin\phi = v\omega_3/g$, the partials that express the sensitivity of $\hat{\phi}(v, \omega_3)$ to the inputs v, ω_3, and to the parameter g are given by

$$\frac{\partial\phi}{\partial\omega_3} = \frac{1}{\omega_3}\tan\phi, \qquad \frac{\partial\phi}{\partial v} = \frac{1}{v}\tan\phi, \qquad \frac{\partial\phi}{\partial g} = -\frac{1}{g}\tan\phi.$$

We also note the partials relating to the sensitivity of $\dot{\psi}$, (recall that $\dot{\psi} = \omega_3\sec\phi$).

$$\frac{\partial\dot{\psi}}{\partial\omega_3} = (1 + \tan\phi)\sec\phi, \qquad \frac{\partial\dot{\psi}}{\partial v} = \frac{\omega_3}{v}\tan^2\phi\sec\phi, \qquad \frac{\partial\dot{\psi}}{\partial g} = -\frac{\omega_3}{g}\tan^2\phi\sec\phi. \tag{E.12}$$

E.2 Steady Motion in a Straight Line

When the motorcycle moves at constant velocity $v = \hat{v}$ in a straight line, $\hat{\phi} = 0$, $\dot{\hat{\phi}} = 0$, $\dot{\hat{\psi}} = 0$, and for convenience, we set $\hat{\psi} = 0$ (i.e., motion is in the x direction). It follows that

$$\delta x = \sum \Phi(\delta r_1 + \delta r_2), \text{ and that } \delta y = \sum -\Phi(\hat{r}_1 + \hat{r}_2)\delta\psi. \tag{E.13}$$

The alignment error $\delta\psi$ evolves according to

$$\delta\psi = \int_0^t \delta\omega_3 dt, \tag{E.14}$$

where we have assumed zero error initially. Replacing $(E.13)_1$ with a continuous time approximation, we find that

$$\delta x = tv\frac{\delta r_1 + \delta r_2}{\hat{r}_1 + \hat{r}_2}, \tag{E.15}$$

and so it is clear that δx grows linearly with time. We expect the error term $\delta\omega_3$ to be random, possibly centered away from 0, and with no overall growth in time. If $|\delta\omega_3|$ was some constant value C (that is, if our prediction of ω_3 was in error only by a constant offset), we would have $|\delta\psi| = Ct$. As it is, we assume that no matter what the nature of $\delta\omega_3$, some constant C exists for which $|\delta\psi| < Ct$. Assuming zero initial error δy we can approximate $(E.13)_2$ by the continuous time integral

$$\delta y = \int_0^t \hat{v}\delta\psi dt. \tag{E.16}$$

Making use of our assumption about the existence of C, we find that $|\delta y(t)| < 0.5\hat{v}Ct^2$. Thus the bound on lateral error grows quadratically with time. In order to have lateral error less than e_y after traveling a distance D at the constant speed $\hat{v}$, the error term $\delta\omega_3$ associated with the signal $\hat{\omega}_3$ must satisfy

$$\left| \int_0^{D/\hat{v}} \delta\omega_3 dt \right| < \frac{2e_y}{D}. \tag{E.17}$$

This equation is useful because it specifies sensor quality as a function of desired navigation performance. Of course, the limitations of this analysis must be kept in mind. When the error terms grow to significant size, nonlinear effects which we have neglected will become important.

E.3 Motion in a circle

We now consider steady circular motion of a motorcycle at the constant speed $\hat{v}$, and with the constant yaw rate $\dot{\hat{\psi}}$. We assume that $\dot{\hat{\phi}} = 0$, and that the motorcycle roll is well approximated by the function

$$\hat{\phi} = \arctan\frac{v\dot{\hat{\psi}}}{g}. \tag{E.18}$$

It follows from (E.6) that $\delta\dot{\psi}$ is given by

$$\delta\dot{\psi} = \sec\hat{\phi}(\dot{\hat{\psi}}\delta\phi + \delta\omega_3), \tag{E.19}$$

and that δx is given by

$$\delta x = \sum \Phi[(\delta r_1 + \delta r_2\cos\hat{\phi} - \delta\phi\hat{r}_2\sin\hat{\phi})\cos\hat{\psi} \; - \delta\psi(\hat{r}_1 + \hat{r}_2\cos\hat{\phi})\sin\hat{\psi}]. \tag{E.20}$$

We note that the symmetry of the motion makes it unnecessary to consider δy. The summation for δx can be approximated by the following integral

$$\begin{aligned}\delta x &= \int_0^t \frac{\hat{v}}{(\hat{r}_1 + \hat{r}_2\cos\hat{\phi})}(\delta r_1 + \delta r_2\cos\hat{\phi} - \delta\phi\hat{r}_2\sin\hat{\phi})\cos\hat{\psi}dt \; - \int_0^t \hat{v}\delta\psi\sin\hat{\psi}dt \\ &= \frac{(\delta r_1 + \delta r_2\cos\hat{\phi} - \delta\phi\hat{r}_2\sin\hat{\phi})}{(\hat{r}_1 + \hat{r}_2\cos\hat{\phi})}\frac{v}{\dot{\hat{\psi}}}\sin\hat{\psi} \; - (\dot{\hat{\psi}}\delta\phi + \delta\omega_3)v\sec\hat{\phi}\left(\frac{\sin\hat{\psi}}{\dot{\hat{\psi}}^2} - t\frac{\cos\hat{\psi}}{\dot{\hat{\psi}}^2}\right),\end{aligned} \tag{E.21}$$

where for convenience we have treated the error terms δr_1, δr_2, and $\delta\phi$ as constants. (A rigorous treatment of these terms would involve the use of bounds such as C in our study of straight line motion). Expressing δx as $A\sin\hat{\psi} + Bt\cos\hat{\psi}$, we see that

$$|\delta x| = |A\sin\hat{\psi} + Bt\cos\hat{\psi}| < |A| + |B|t. \tag{E.22}$$

Hence in steady circular motion, the x and y bounds on position error grow linearly with time. Recall that for steady straight line motion, the bound on position error in the direction of motion grows linearly with time but that the bound on position error transverse to the direction of motion grows quadratically with time. The relationship between maximum allowable error and sensor performance depends on the fastest growing error bound for a standard motion, and so it is pointless to develop an expression of the form (E.17) from our analysis of steady motion in a circle.

References

[1] Brown, R. G., Hwang, P. Y. C. *Introduction to Random Signals and Applied Kalman Filtering.* Third edition, John Wiley & Sons, 1997, ISBN 0471128392

[2] Britting, Kenneth R. *Inertial Navigation Systems Analysis.* 1971. John Wiley and Sons, Inc. ISBN 047110485

[3] Cossalter, V. *Motorcycle Dynamics.* Race Dynamics. Greendale, WI. 2002. ISBN 0972051406

[4] Cossalter, V., Dalio, M., Lot, R., and Fabbri, L. "A General Method for the Evaluation of Vehicle Manoeuvrability with Special Emphasis on Motorcycles." *Vehicle System Dynamics.* Vol. 31. pp113-135 1995

[5] Cossalter, V. and Lot, R. "A Motorcycle Multi-Body Model for Real Time Simulations Based on the Natural Coordinates Approach." *Vehicle System Dynamics.* Vol. 37. No. 6. pp.423-447. 2002.

[6] Farrell J.A., Barth M. *The Global Positioning System & Inertial Navigation.* McGraw-Hill, New York, NY, 1999, ISBN 007022045X

[7] Heckermann, E.W., Roche, G.W., and Dance, F.J. "The BMW On-Board Navigation System" *Society of Automotive Engineers* Paper 972640. 1997.

[8] Hedrick, K., O'Reilly, O.M., Coaplen, J., Kessler, P., *The Development of an Inertial Measurement Unit and a Human-Machine Interface for Motorcycle Navigation Systems.* Department of Mechanical Engineering, University of California at Berkeley, January 2004.

[9] Jutkowitz, A. J., *On Inertial Navigation of a Motorcycle Using a Limited Number of Sensors.* Masters of Science Report, Department of Mechanical Engineering, University of California at Berkeley, May 2003.

[10] Lawrence, A. *Modern Inertial Technology.* 1993. Springer-Verlag New York, Inc. ISBN 0387978682

[11] Maybeck, Peter S. *Stochastic Models, Estimation and Control.* vol. 1. Academic Press, 1979 ISBN 0124807011

[12] McGuan, S.P. "Active Human Surrogate Control of a Motorcycle: Stabilizing and De-Stabilizing." *Society of Automotive Engineers* Paper 930226. 1993.

[13] O'Reilly, O.M. *Engineering Dynamics, A Primer.* Springer 2001. ISBN 0387951458

[14] Sharp, R.S. "The Stability and Control of Motorcycles." *Journal of Mechanical Engineering Science.* Vol. 13, No. 5. 1971

[15] Sharp, R.S. and Limebeer D.J.N. "A Motorcycle Model for Stability and Control Analysis." *Multibody System Dynamics.* Vol. 6. pp123-142. 2001

[16] Stevens, D. *The Influence of Roll Dynamics on Motorcycle Navigation Systems.* University of California at Berkeley. M.S. Thesis. 2002.

[17] Turetzky, G., Chansarkar, M., and Gehue, H. "GPS as the Primary Navigation Sensor for ITS." *Navigation and Intelligent Transportation Systems.* Warrendale, PA. Society of Automotive Engineers. 1998.

[18] Weir, D.H. *Motocycle Handling Dynamics and Rider Control and the Effect of Design Configuration on Response and Performance.* University of California at Los Angeles. Ph.D. Thesis. 1973.

[19] Wei-Wen, K. "Integration of GPS and Dead-Reckoning Navigation Systems." *Vehicle Navigation & Information Systems Conference proceedings.* Vol. 2. Warrendale, PA. Society of Automotive Engineers. 1991.

[20] ADAMS v11 Documentation "Using ADAMS/Solver - Using Tire Statement" pp. 935 – 1036. Mechanical Dynamics, Inc. Ann Arbor, MI. 2000.